DSD Variations on Rain-Rate Estimate Algorithms of X-Band Polarimetric Radar and Rainfall Characterization in Tropical Environments Using 2DVD, Rain Gauges and TRMM Data

by

Margarita Baquero Fuentes

A thesis submitted in partial fulfillment of the requirements for the degree of

MASTER OF SCIENCE
in
ELECTRICAL ENGINEERING

UNIVERSITY OF PUERTO RICO
MAYAGÜEZ CAMPUS
2005

Approved by:

_____	_____
Sandra L. Cruz-Pol, PhD President, Graduate Committee	Date
_____	_____
José Colom Ustáriz, PhD Member, Graduate Committee	Date
_____	_____
Henrick M. Ierkic-Vidmar, Ph.D Member, Graduate Committee	Date
_____	_____
Wolfgang Rolke, PhD Representative of Graduate Studies	Date
_____	_____
Isidoro Couvertier, PhD Chairperson of the Department	Date

ABSTRACT

Data from NASA TRMM satellite and rain gauges, the rain rate per hour was studied. The comparison took place in San Juan, Puerto Rico; when the Tropical Storm Jeanne passed over the island of Puerto Rico.

Natural variations in raindrop size distribution (DSD) were studied for X band radar from October 2004 to July 2005 and September 15^{th} to 16^{th}, 2004 in San Juan, Puerto Rico. Three types of estimators of rain rates were examined: A classical estimator $R(Z_H)$ and two polarimetric radar estimators $R(K_{DP})$ and $R(Z_H,Z_{DR})$. According to simulation results, the normalized errors (NEs) with respect data disdrometer of $R(Z_H)$,$R(K_{DP})$ and $R(Z_H,Z_{DR})$ for all DSD samples in October 2004 to July 2005 data are 40.85%, 14.73%, and 15.83% respectively, while for the tropical storm Jeanne they are 23.39%, 9.35% and 14.53%. The results show that the estimator $R(Z_H)$ is the most sensitive to variations in DSD.

To my mom, my niece, my family and Diego …

ACKNOWLEDGEMENTS

Many people have helped me in the course of my research, and any merit in it is in large measure due to them.

At the University of Puerto Rico, first and foremost, I gladly acknowledge my debt to Dr. Sandra Cruz-Pol who gave me the opportunity to undertake graduate studies overseas while becoming part of a great research team with her supervision. Without her constant friendship, confidence, encouragement and advice over these two years, this thesis would never been completed.

Dr. José Colom provided me with the sound and advance knowledge on Electromagnetic needed to succeed with this project. I am so grateful with these two professors. Not only has my academic knowledge grown with their guidance, but also my perception about life.

Dr. H. Mario Ierkic for serving on my graduate committee and for his support, understanding and bright ideas through out my research. His judgment gave me different point of views I would have not considered otherwise.

At the Colorado State University (CSU), special thanks I owe to Dr. V.N. Bringi for clarifying my mind on the path to this thesis while taking his course on Polarimetric Doppler Weather Radars.

Dr. V. Chandrasekar, for the chance of having the video disdrometer installed in Puerto Rico for more than one year, and Miguel Gálvez, who taught me so many things about it.

I would also like to thank NWS local WFO personnel, Israel Matos, Bert Gordon, Wilfredo Muñoz, Marlon Carter, and especially to Rachel Gross. Without their help and support, the dream of having a working disdrometer in Puerto Rico would not have been possible.

For financial support, I would like to acknowledge the Electrical and Computer Engineering Department from the University of Puerto Rico and its NASA research centers, Cloud Microwave Measurements of Atmospheric Phenomena (CLiMMATE) and the Tropical Center for Earth and Space Studies (TCESS). The funding and resources for the development of this research were provided under Faculty Awards for Research NAG-1-02074 and University Research Center grant NCC5-518 respectively; TCESS primarily supported this work. This work also made use of CASA Engineering Research Center Shared Facilities supported by the National Science Foundation under Award Number 0313747.

I want to thank my friends for your support during graduate school. Special thanks to José Maeso, Pablo Rebollo, Jorge Trabal, Víctor Marrero, Mauricio Sánchez and José Morales.

The work in this project has been greatly supported by my beloved family. I express my sincere gratitude to my parents Elisio and Margarita, from whom I am, hopefully,

starting to learn the prosperities of life; and my niece Sofia, for her cuteness and friendship; Eliseo and Liliana, for their long-distance support, and also, merely for being my brother and sister.

Finally, I deeply thank God for giving me the opportunity to enrich myself with the Puerto Rican culture throughout this experience, and especially His bless having met the Mari family, who gave me all their support during this journey.

Table of Contents

Table List

Tables **Page**

Figure List

Figures **Page**

1 INTRODUCTION

The goal of this work was to calculate the expected rain rate outcome from an X-band radar by using a disdrometer data. Our objective was to find different equations relating rain rate (R) and polarimetric radar parameters. Furthermore, this work also includes the analysis of how sensitive is the computed rain rate to Specific Differential Phase (K_{dp}) for different frequencies.

Upon installation of the radars for the Collaborative Adaptive Sensing of the Atmosphere (CASA) project, the required calibration was made by comparing Two-Dimensional Video Disdrometer (2DVD), Tropical Rainfall Measurement Mission (TRMM) and National Climate Data Center (NCDC) data through the codes developed along with the present work.

1.1 Motivation

Precipitation is an important meteorological parameter which affects the hydrology of land surface, coastal processes, terrain stability, climate and global heat circulation. Understanding rainfall distribution and intensity can improve protection of environmental and human resources, and knowledge of geophysical process of land, ocean and atmosphere.

Rain measurements have been historically verified using traditional rain-gauges in high detail or microwave radars that cover vast areas. Nevertheless, in order to develop

more accurate rainfall forecast algorithms and validate them, the drop size distribution (*DSD*) of rainfall events needs to be studied.

The quantitative estimation of rainfall rates using meteorological radars has been one of the main research topics in radar meteorology and radar hydrology. Quantitative Precipitation Estimation (QPE) pursues to improve the precipitation estimates and enhance the reliability of flood prediction. Developing low cost radar is one of the key goals of this research enterprise.

The relationship between rain rate R and the radar reflectivity factor Z (Z-R relations) have been widely used to estimate rainfall amounts. However, it is commonly recognized that this classical rain estimation method has many sources of error. One of them is the sensitivity of Z-R relations with respect to variations in raindrop size distributions (*DSD*)[*Maki* and *Bringi*, 2004].

For shorter wavelengths in comparison with S-band, such as X-band (3 cm) and C-Band (5 cm), attenuation by rainfall is an additional source of error for quantitative rainfall estimation, it was found by Battan, 1973. It has been recognized for a long time that the X-band wavelength was not useful for accurate rainfall measurements because of the rain attenuation problem of Z_h. However, this situation changed dramatically after polarimetric radars, which measure Differential Phase, became available. The Differential Phase is not very sensitive to DSD specific parameters, it is independent of radar calibration problems and, in addition, it is also immune to rain attenuation. Note that radar power calibration is usually difficult and is one of the major sources of signal power measurement errors.

The raindrop distribution is generally assumed to be uniform within the radar sampling volume; however, gradients within the sampling volume can cause overestimation or underestimation of rain rates. Contamination by hail and the bright band is one of the well-known sources of bias error. To infer intrinsic meteorological parameters from the measurement in X-Band, accurate correction for attenuation is critical *Maki* and *Bringi*, 2004.

The Collaborative Adaptive Sensing of the Atmosphere (CASA) Engineering Research Center (ERC) aims to create a new engineering paradigm in observing, detecting and predicting weather and other atmospheric phenomena. Developing low cost radars is one of the key goals of this research enterprise. This can be accomplished by moving to higher frequencies, specifically X-Band. More information can be found on the CASA webpage.

A radar calibration method that has been widely used in operations employs radar-rain gauge comparison. It is referred to as an adjustment rather than a calibration. In the simpler version of the method, observed radar reflectivities are transformed into rainfall rates, using a single or several *R-Z* relationships $Z = aR^b$, and these rates are compared to rainfall rates observed by one or several rain gauges.

Using measurements from NASA TRMM satellite webpage and rain gauges, the raindrop size distribution was studied and used in analyzing disdrometer rain retrieval. The data used for this comparison two events which; September 2004 (when the tropical storm Jeanne passed by the island of Puerto Rico). Only 4 out of 21 locations worldwide

where 2DVDs have been deployed in the past are in the tropics, therefore this work provides further insight into the rainfall statistics of tropical regions.

In order to evaluate the currently used algorithms for rain estimation, we performed a data comparison and correlation between NCDC (National Climate Data Center) rain gauge, NWS rain gauge, a 2DVD and NASA TRMM. This helped in the characterization of this tropical island's rainfall rate statistics and its regional variations. The results of this work should provide important information for QPE algorithms for enhanced rainfall estimation, much needed for the tropical zone communities.

1.2 Literature Review

In recent years, polarimetric radar techniques have been evolving quickly and its achievements have become the center of attention of the meteorology community. Radar meteorology, traditionally use *Z-R* relations to estimate rain rates, whereas polarimetric radar uses both *Z* and polarimetric variable information such as specific differential phase K_{DP} and/or differential reflectivity Z_{DR}. *Seliga and Bringi* (1976) showed that Z_{DR} could be used to retrieve rain drop size distributions and to improve rain rate estimations was proposed theoretically (e.g., *Oguchi* and *Hosoya* 1974 , and *Seliga* and *Bringi* 1976) and now is recognized as an essential parameter for polarimetric radar measurements. Comparisons of radar rain rate estimates with gauge measurements have often been performed to asses the accuracy of radar rate rain estimators. *Matrosov* et al. (2002) showed that case tuned $R(Z_H)$ was a more accurate estimator than $R(K_{DP})$ by comparing the X-band polarimetric radar estimates with gauges measurements.

Advantages of K_{DP} based estimators are that they are not affected by radar calibration errors or partial beam occlusion, and are less susceptible to ground clutter effect (*Vivekanandan* et al. 1999; *Zrnic´ and Ryzhkov* 1996). As shown in those studies, the differential phase shift at S-band is characterized by relatively low sensitivity to rainfall rate, which impacts the resolution of rain products derived from K_{DP} estimators. Consequently, the use of X-band wavelengths should allow more detailed and potentially more accurate estimation of light to moderate rainfall rates.

There are two main complications in using polarimetric parameters (Z_{DR} and K_{DP}) at X-band that require careful investigation: 1) the presence of drop size distribution effect in cases of significant concentration of large drops, and 2) the variability in raindrop size distribution and in the equilibrium relationship between oblate raindrop shape and size. *Zrnic´* et al. (2000) and *Keenan* et al. (2001), who studied the sensitivity of C-band polarimetric variables to the form of raindrop axial ratio and the tail of raindrop size distribution, have exemplified the effect of both issues on the accuracy of rainfall estimation. Currently, research on the use of polarimetric radar measurements at X-band has been limited to a few theoretical (*Jameson* 1994, 1991; *Chandrasekar* and *Bringi* 1988; *Chandrasekar* et al. 1990) and experimental studies (*Tan* et al. 1991; *Matrosov* et al. 1999; *Matrosov* et al. 2002).

The experimental study by *Matrosov* et al. (1999), although valuable from the viewpoint of polarimetric techniques development, did not provide adequate quantitative evaluation of the estimators. In their most recent study, however, *Matrosov* et al. (2002) provided a quantitative error analysis of the various rain estimators based on field data.

They concluded that a multi-parameter algorithm consisting of Z_H, Z_{DR}, and K_{DP} measurements provides the least standard error compared to other single-parameter estimators. According to the authors, the combined polarimetric parameter algorithm intrinsically accounts for the variability in equilibrium drop shape–size relationship, thus offering a more stable estimator.

Anagnostou et al. 2004, show that the multiparameter (Z_H, Z_{DR}, and K_{DP}) retrieval has the optimum rain estimation performance with about 40% relative difference standard deviation. For comparison, the case-tuned reflectivity–rainfall rate *(Z–R)* relationship gave about 65% relative difference standard deviation.

More recent studies (e.g., *Brandes* et al. 2001) showed, however, that rainfall estimates obtained with a fixed coefficient K_{DP}–R relation are similar to those obtained from the radar reflectivity only given that the radar is well calibrated.

Maki, Park and Bringi 2005, conclude that the estimator $R\ (K_{DP})$ is less sensitive to natural variations in DSD than the classical estimator $R(Z_H)$ and calculated relationships for convective rain, stratiform rain and all rain types, as show in Table 1-1.

Table 1-1. Relationships for rain rate estimator Darwin, Australia (*Maki* et al 2005).

Equation	Rain type	c	b	
$R(Z_{H)} = cZ_H^{\ b}$	Convective	4.26×10^{-2}	0.644	
	Stratiform	3.96×10^{-2}	0.551	
	All	**9.16×10^{-3}**	**0.770**	
$R(K_{DP}) = c_1 K_{DP}^{\ b_1}$	Rain type	c_1	b_1	
	Convective	20.2	0.809	
	Stratiform	14.5	0.811	
	All	**18.9**	**0.856**	
$R(K_{DP}, Z_{DR}) = c_2 K_{DP}^{\ a_2} 10^{0.1 b_2 Z_{DR}}$	Rain type	c_2	a_2	b_2
	Convective	25.1	0.893	-1.03
	Stratiform	23.9	0.881	-1.39
	All	**25.2**	**0.916**	**-1.14**

$R(Z_H, Z_{DR}) = c_3 Z_H^{a_3} 10^{0.1 b_3 Z_{DR}}$	Rain type	c_3	a_3	b_3
	Convective	1.01 x10^{-2}	0.913	-4.92
	Stratiform	1.49 x10^{-2}	0.855	-4.83
	All	**8.99 x10^{-3}**	**0.927**	**-5.05**

Additionally, the estimators of rain rate derived from disdrometer data collected in Tsukuba, Japan are show in Table 1-2.

Table 1-2 Relationships for rainrate estimator Tsukuba, Japan (*Maki* et al 2005).

Equation	Rain type	c		b
$R(Z_h) = cZ_h^b$	All	0.0394		0.619
$R(K_{DP}) = c_1 K_{DP}^{b_1}$	Rain type	c1		b1
	All	19.6		0.825
$R(K_{DP}, Z_{DR}) = c_2 K_{DP}^{a_2} 10^{0.1 b_2 Z_{DR}}$	Rain type	c2	a2	b2
	All	26.0	0.883	-0.0988
$R(Z_H, Z_{DR}) = c_3 Z_H^{a_3} 10^{0.1 b_3 Z_{DR}}$	Rain type	c3	a3	b3
	All	0.130	0.869	-0.429

The normalized errors (NEs) of $R(Z_H)$ and $R(K_{DP})$ are 25% and 14%, respectively.

Figure 1-1 shows the comparison with two different locations (Darwin Australia and Tsukuba, Japan) where the relation R-K_{DP} have difference in less than 5% while the comparison of the R-Z_H relationship between Darwin and Tsukuba shows that the average difference without regard for sign is about 77%. For this reason $R(K_{DP})$ is less sensitive to DSD variations compared to $R(Z_H)$ and supports the conclusion of *Bringi*, 2003.

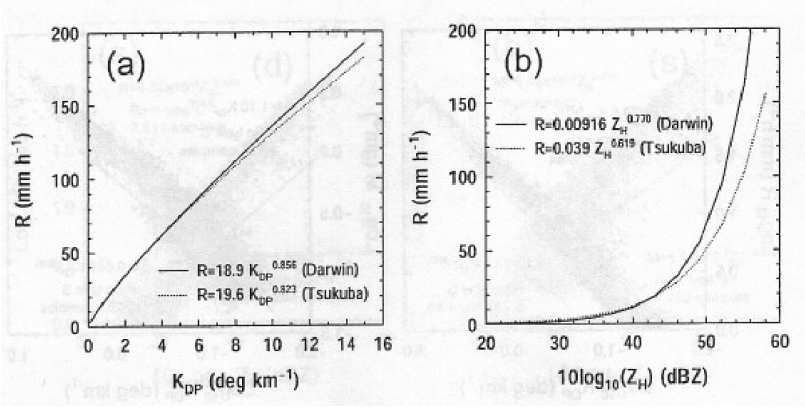

Figure 1-1. The dependence of rain estimators on geographical location ; (a) the R-K_{DP} relationship and (b) the R-Z_H relationship, *Maki, Park* and *Bringi*, 2005.

One advantage of the X-band wavelength compared to S-Band and C-Band wavelengths is its sensitivity of differential phase to rain rate. Figure 1-2 shows the dependence of the relationship between K_{DP} and R on the wavelength, the increase in sensitivity of K_{DP} is remarkable at X-Band wavelength. K_{DP} value is more than 3 times larger than that at S-Band wavelength and about two times larger than at the C-Band wavelength for the same rain rate (this is due to the inverse dependence of K_{DP} with wavelength [*Bringi* and *Chandrasekhar*, 2001].

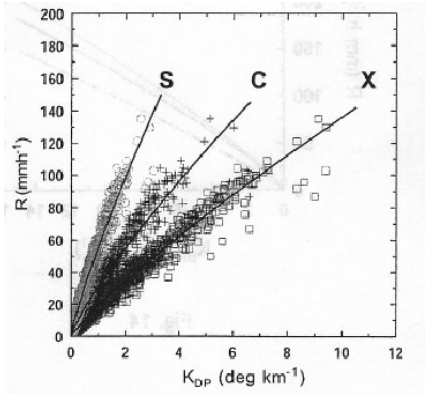

Figure 1-2. Dependence of R-K_{DP} relations on wavelength, *Maki* and *Bringi*, 2005.

In addition, *Sachidananda and Zrnic* 1987, and Jameson 1991 found that accuracies of 0.1dB are necessary for Z_{DR} measurements, and at least 0.5dB accuracy for Z_H measurements are necessary for accurate estimation of rain rates.

Radar reflectivity factor (Z_H), differential reflectivity (Z_{DR}), and specific differential phase (K_{DP}) as determined from radar measurements and computed from disdrometer observations were compared for long-lived events occurring on 8 and 20 August and 17 September by *Brandes* et al, 2002. On average, the disdrometer reflectivity values were 0.20 dB higher than that measured by radar. Differential reflectivity values averaged 0.25 dB larger than those measured with radar. This difference is much bigger than bias errors found by tilting the radar antenna vertically; hence, the basic radar measurement is not the source of the discrepancy. The difference is within the range of values and similar in sign to the studies of *Goddard* et al. (1982), *Goddard and Cherry* (1984), *Chandrasekhar* et al. (1988), and *Andsager* et al. (1999). As concluded by these investigators, the discrepancy is thought to originate with drop oscillations resulting in mean shapes that are more spherical than the equilibrium values.

2 Theory

Rainfall data was classified between convective and stratiform rain using the gamma function. The present study uses a least square fitting method to estimate the three parameters N_0, Λ, μ of gamma DSD.

2.1 Gamma Distribution

A continuous random variable x is said to have a gamma distribution if the range of x consists of all positive real numbers and if *x* possesses a density function *f(x)* that satisfies the equation

$$f(x) = \frac{1}{\beta\Gamma(p)}(x/\beta)^{p-1}e^{-x/\beta} \qquad \textbf{2.1}$$

Where β and *p* are positive numbers and $\Gamma(p)$ is the gamma distribution. The mean of the density function is *p*, and the standard deviation is $\Gamma(p)$. The gamma distribution is skewed to the right.

$$\Gamma(p) = \int_0^\infty t^{p-1}e^{-1}dt \qquad \textbf{2.2}$$

In meteorology, scalar multiples of gamma distribution are used to represent size distributions of clouds drops.

2.2 Gamma Drop Size Distribution

The general form of gamma is used to study natural variations of DSD.

$$N(D) = N_0 D^{\mu} e^{(-\Lambda D)} = N_0 D^{\mu} e^{\left[\frac{(3.67+\mu)}{D_0} D\right]} \quad \textbf{2.3}$$

where *N(D)* is the number of drop, *D* is the diameter, N_0 is the intercept parameter and μ controls the shape of the DSD, Λ is the slope parameter of the resulting straight line.

$$N_0 = 10^3 \frac{\Lambda^4 M}{\pi \rho_w} = \frac{10^3 (3.67)^4}{\pi \rho_w} \left(\frac{M}{D_0^4}\right) \quad \textbf{2.4}$$

$$\Lambda = \frac{(3.67 + \mu)}{D_0} \quad \textbf{2.5}$$

$$\Lambda D_m = 4 + \mu \quad \textbf{2.6}$$

$$D_m = \frac{4 + \mu}{3.67 + \mu} D_0 \quad \textbf{2.7}$$

N_w (in $mm^{-1}m^{-3}$) is an "intercept" parameter defined as

$$N_w = \frac{(3.67)^4}{\pi \rho_w} \left(\frac{10^3 M}{D_0^4}\right) \quad \textbf{2.8}$$

where *M* is the water content.

The mass weighted mean diameter (D_m) of the DSD is defined by

$$D_m = \frac{\int D^4 N(D) dD}{\int D^3 N(D) dD} \qquad \textbf{2.9}$$

The data from the rain events can be normalized using

$N(D)/N_w$ and D/D_m

The normalization reduces the scatter in the data and is useful in comparing the shapes of distributions with widely different rain rates.

The conversion of radar reflectivities to rainfall parameters uses standard models for DSDs [*Schönhuber*, 1995], such as the well known Marshall-Palmer DSD (MP-DSD), and others as the Joss-Drizzle (JD-DSD), and the Joss-Thunderstorm (JT-DSD) models [*Schönhuber*, 2000]. These three are exponential models of the form

$$N(D) = N_0 e^{-\Lambda D} \qquad \textbf{2.10}$$

where N_0 is the scaling factor and is fixed to 8,000, 30,000 and 1,400 /m^{3}mm respectively, for the models mentioned above, and Λ is a function of the rainfall rate and. The parameter Λ of the exponential distribution that fits the MP-DSD is $4.1R^{-0.21}$ mm^{-1} when the rainfall rate is in millimeters per hour. Although MP-DSD is very popular in computing rainfall rates derived from radar reflectivities measurements, actual drop sizes change significantly by geographic location, type of storm, season, and region within the storm. Regarding tropical climates, all three models mentioned produce huge overestimations of rainfall rates [*Schönhuber*, 2000].

2.3 Rain Rate and Rain Water Content

To estimate rain that will fall over a certain area, the rain-rate is derived from the DSD and the drop's diameter and terminal velocity, as shown *by Kruger and Krajewski* (2001) and by *Doviak and Zrnić* (1993). The relation of these parameters is

$$R = \frac{\pi}{6}\int_0^\infty D^3 N(D) v_t(D) dD \qquad \textbf{2.11}$$

where R is rainfall rate in mm•hr^{-1}, D and v_t are the drop's diameter and terminal velocity in mm and m•s^{-1} respectively, and $N(D)$ is the DSD. Accurate measurements of these quantities are consequently needed. Both diameters and terminal velocities of falling hydrometeors can be obtained from the 2DVD accurately as demonstrated in [*Kruger*, 2001], and [*Schönhuber*, 1995, 2000]. The 2DVD software arranges drop information to construct DSD, according to *Kruger*.

Atlas et al. (1973) came up with a useful formula to calculate terminal velocities of water droplets that produces less than 2% error from precise measurements made by *Gun and Kinzer* (1949), if the diameter of the drops is between 0.6 and 5.8 mm. This formula is the one used by the 2DVD to compute drops' vertical velocities, and is expressed as

$$v_t(D) = 9.65 - 10.3e^{(-0.6D)} \text{ m/s} \qquad \textbf{2.12}$$

when D is in mm. The aforementioned velocities measurements were performed in stagnant air. For the 2DVD, low-wind conditions are necessary in order to obtain

accurate and detailed information on drop size, velocity, and shape. A high-wind condition introduces errors in the instrument readings.

The rain water content M (kgm^{-3}) is one of the most important parameters in meteorology where the vertical integrated liquid water content (VIL) is a useful parameter for very short-range forecasting of rainfall. On larges scales, the changes in M with height over long periods of time is related to the latent heat release in the surrounding atmosphere, which is an important heat source in global-scale circulation[*Maki* and *Bringi*, 2005], M is given by

$$M = \frac{\rho_w \pi}{6} \int_0^{D_{\max}} D^3 N(D) dD \qquad \textbf{2.13}$$

ρ_w is the water density ($=10^3$ kgm^{-3}) or

$$M = 10^{-3} \pi \rho_w \int_0^{\infty} D^3 N_0 \exp(-\Lambda D) dD = 10^{-3} \frac{\pi \rho_w N_0 \Gamma(4)}{6\Lambda^4} \qquad \textbf{2.14}$$

Where ρ_w is 1 g cm^{-3}, D is in mm and N_0 in $mm^{-1}m^{-3}$.

2.4 Drop Shape

Assuming that the air flow is steady, the equilibrium shape of a raindrop is determined by a balance of forces on the interface involving hydrostatic, surface tension, and aerodymanic forces.

Axis ratio is defined as *b/a*, with *b* being the semi-minor axis length and *a* the semi-major axis length; see Figure 2-1.

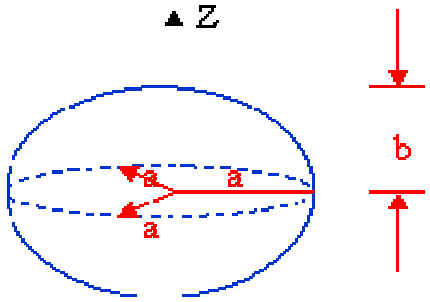

Figure 2-1.An oblate spheroid with symmetry axis along de Z-axis.

The axis ratio formulae used in the present study for static shape of drops is for equilibrium axis ratios derived from the numerical model of *Beard and Chuang* (1987), and is expressed as

$$\frac{b}{a} = 1.0048 + 0.0057\left\{\frac{D}{10}\right\} - 2.628\left\{\frac{D}{10}\right\}^2 + 3.682\left\{\frac{D}{10}\right\}^3 - 1.677\left\{\frac{D}{10}\right\}^4 \quad D > 0.3 \text{ mm} \qquad \textbf{2.15}$$

For *D* from 1 to 6 mm, Figure 2-2 show the equilibrium shapes using the numerical model of *Beard and Chuang* (1987), who included aerodynamic effects.

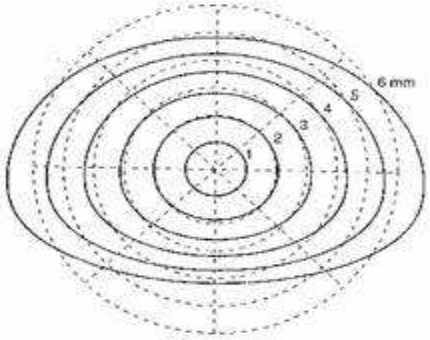

Figure 2-2 Equilibrium drop shapes for drop diameter of 1-6 mm. From *Beard and Chuang* (1987).

2.5 Polarimetric parameters

The reflectivity factor for horizontal (H) polarization (mm^6m^{-3}) is defined by

$$Z_H = \frac{\lambda^4}{\pi^5}\left|\frac{m^2+1}{m^2-1}\right|^2 \int_0^{D_{\max}} \sigma_{bH}(D)N(D)dD \qquad \textbf{2.16}$$

λ is the radar wavelength, m is the complex refractive index of water, σ_{bH} the backscatter cross section for horizontal polarization.

Differential reflectivity Z_{DR} is the ratio between the horizontal and vertical reflectivity; it is very useful for discriminating large drops from hail and to determine rain rates independent of the drop-size distribution; since it only depends on the axial ratio. In order to measure Z_{DR}, a dual-polarized radar system is required [*Bringi* and *Chandrasekar*, 2001].

The differential reflectivity Z_{DR} (dB) is defined by

$$Z_{DR} = 10\log(\frac{Z_H}{Z_V}) \qquad \textbf{2.17}$$

The differential reflectivity Z_{DR} is a measure of the reflectivity-weighted mean axis ratio of the hydrometeors in a radar sampling volume which is defined by the radar beam width and the pulse width [*Maki* and *Bringi*, 2005].

The specific differential phase K_{DP} (deg km^{-1}) is the difference between propagation constants for horizontally- and vertically- polarized radar pulses over a given range which is much more directly related to the DSD and rain rate than either Z or Z_{DR}, particularly in heavy rain, and is defined by

$$K_{DP} = \frac{180}{\pi}\lambda \,\mathrm{Re}\left\{\int_0^{D_{\max}} [f_H(D) - f_V(D)]N(D)dD\right\} \quad \textbf{2.18}$$

Where Re{} refers to the real part of the integral, f_H and f_V are the forward-scattering amplitudes for horizontal (H) and vertical (V) polarizations, respectively (*Oguchi* 1983).

The differential phase shift (deg) is defined by

$$\phi_{DP} = 2\int_0^r K_{DP}\,dr + \delta \quad \textbf{2.19}$$

In where r is the range and δ is the backscatter phase shift, caused by non-Rayleigh scattering.

2.6 Error

To quantitatively examine the uncertainty in the rain estimators three types of error were calculated; the normalized error (NE), the percentage root-mean squared error (PRMSE), and the maximum relative error (MRE). These errors are defined as:

$$NE = \left\langle \left| R_{est} - R_{dis} \right| \right\rangle / \left\langle R_{dis} \right\rangle \quad \textbf{2.20}$$

$$PRMSE = \left\langle \sqrt{(R_{est} - R_{dis})^2} \,/\, R_{dis} \right\rangle \quad \textbf{2.21}$$

$$MRE = \left[(R_{est} - R_{dis}) / R_{dis} \right]_{\max} \quad \textbf{2.22}$$

where, $\langle\ \rangle$ means the average for a certain interval and $[\ ]_{\max}$ means the maximum value of the relative error observed in each range.

3 Equipment Description

In order to evaluate current algorithms for rain estimation, we performed a data comparison and correlation between NCDC rain gauges, NWS rain gauge, a 2DVD and NASA TRMM. Furthermore, this will help in the characterization of this tropical island's rainfall rate statistics and its regional variations. The results of this work present important information for QPE algorithms for enhanced rainfall estimations much needed for the tropical zones communities. Upon installment of CASA radars, the required calibration will be made by comparing 2DVD, TRMM and NCDC data through the codes developed along with the present work.

3.1 Rain gauges

Puerto Rico is sampled by several rain gauge networks with over 170 reporting stations combined.

The Federal Aviation Administration (FAA) has put in place an Automated Surface Observing System / Automated Weather Observing System (ASOS/AWOS). The rain gauge used in this work is of the Automated Surface Observing System (ASOS) type with an ATIS interface, which is shown in Figure 3-1(a). Such an interface allows ASOS weather observations to be appended to the ATIS broadcast, thereby providing real-time weather when the tower is closed. Upon closing part-time towers in the evening, the controller has the ability to add overnight ATIS information to the ASOS automated voice weather message. When the tower is open the pilots get ATIS information and the hourly weather. When the tower is closed, the pilots get the one-minute weather

information along with the ATIS information on the same frequency. This approach allows the pilot to utilize the same frequency 24 hours a day to obtain weather information. An ASOS processes and outputs cloud height/condition temperature, dew point, barometric pressure, density altitude, wind speed, wind direction, and gusts plus a freezing rain sensor and thunderstorm reporting.

(a)

Time	Precipitation
1	0.01
2	0
3	0
4	0
5	0.01
6	0
7	0
…	…
23	0.04
24	0

(b)

Figure 3-1ASOS_ATIS. (a) Photo and (b) fragment of its data format.

This station is monitored constantly by the NWS office and archived at National Climate Data Center (NCDC). These data were used to validate and compare 2DVD measurements. Figure 3-1(b) shows a fragment of text-file containing precipitation information gathered at this station.

3.2 TRMM

NASA TRMM (Tropical Rain Measurement Mission). TRMM includes the first space-borne precipitation radar (PR) designed to provide three-dimensional maps of storm structure. It was launched on November 28, 1997. Its circular orbit altitude is 350

km with 35 deg of inclination. It has an orbit duration of 91 minutes (16 orbits a day), spending 1.14 minutes over Puerto Rico during each orbit and 18.2 minutes each day.

The TOVAS website provides TRMM data in text format in addition to rain rate pictures, as shown in Figure 3-2.

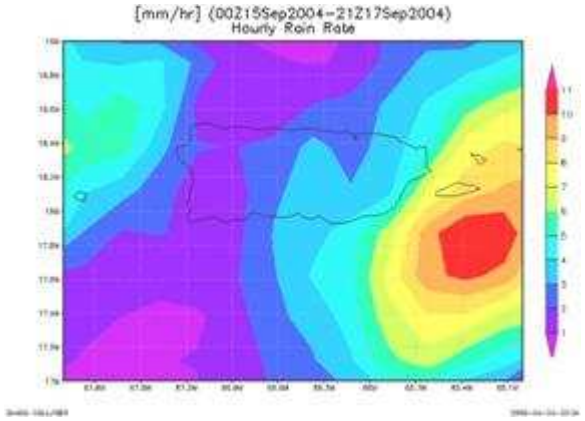

(a)

TRMM 3B42RT 3-Hourly Precip. Product
Selected parameter: Hourly Rain Rate
Selected area: lat=[18.0,18.25], lon=[-66,-65.75]
Selected time period: (00Z30Jan2005-15Z30Jan2005)
Undefined/Missing Value: -99999

Latitude	Longitude	Hourly Rain Rate(mm/hr)
18.000	-66.000	0.0267
18.000	-65.750	0.0383
18.250	-66.000	0.0217
18.250	-65.750	0.0283

(b)

Figure 3-2(a) TRMM picture and (b) data format for Tropical Storm Jeanne, Sept 2004.

With the goal of comparing 2DVD data with each one of the other sensors (TRMM and NCDC), separate analyses were made, comparing TRMM against 2DVD and NCDC against 2DVD. The comparison took place with data collected from September 15th through 16th, 2004, in which the tropical storm Jeanne passed over Puerto Rico. The root-mean-squared (RMS) error was computed for each case.

Differences in the data between the devices were handled prior any comparison was made, and as taken into account in the conclusions of such comparisons. Data from NCDC rain gages is measured in inches, and in local AST time, whereas 2DVD data is

obtained every minute, and is given in millimeters and UT time. TRMM data from NASA TOVAS is averaged every 3 hours, given in millimeters and UT time. Furthermore, TRMM was corrected by location by identifying an area over the 2DVD's position. A Matlab tool was developed in order to resolve any data conversion issues between these data sources as well as additional computations needed.

3.3 Two Dimensional Video Disdrometer(2DVD)

The 2DVD was developed by Joanneum Research from Graz, Austria, and the ESA/ESTEC (European Space Agency / European Space and Technology Centre). Joanneum Research, with 15 research units, is one of the largest non-university research institutions in Austria. Additionally, students of the Technical University of Graz have also contributed to its development.

A 2-dimensional video disdrometer (2DVD) records orthogonal image projections of raindrops as they cross its sensing area, and can provide a wealth of information, including velocity and shape, of individual raindrops. 2DVDs have been deployed in 21 locations around the world; a prototype has recorded data as early as 1992. Although it can take measurements from rain, snow, and mixed precipitation, it will be used for rain only, as it is deployed in the tropical island of Puerto Rico. Prior to this work the 2DVD has been deployed in 4 other locations within the tropics.

3.3.1 Sensor Unit

The Sensor Unit houses the two cameras, two light sources, and several mirrors. Mirrors are used to deflect light as lamps are not directly in front of the cameras. Each

camera-lamp pair is orthogonal to the other, providing the two-dimensional aspect of the measurement.

When a raindrop falls into the measuring area, cameras 1 and 2 detect the drop shadow as shown in Figure 3-3. The two orthogonal projections provide 3D raindrop shape information that is used to describe the raindrop. The sensor unit operates at a frequency of 34.1 kHz, taking drop measurements every 29 microseconds approximately.

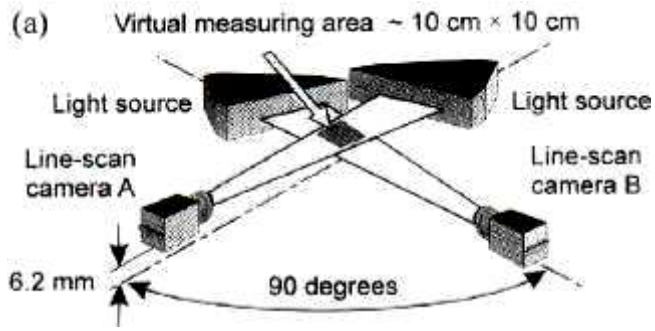

Figure 3-3. Sketch of Sensor Unit components [*Schönhuber*, 1994].

3.3.2 Outdoor Equipment Unit (OEU)

The OEU consists of an embedded computer (PC), power supply – to power lamps and cameras – and connections for power and video signals from the cameras. It receives those video signals from cameras, pre-processes raw data, and runs software for data acquisition and plane alignment. It also provides connections for a keyboard and monitor to access its computer.

3.3.3 Indoor User Terminal (IUT)

The IUT is a regular PC that receives the pre-processed data from the OEU and performs the final computations. It also provides display of these calculations via a

proprietary software called VIEW_HYD. An image of the software display is shown in Figure 3-4. IUT is commonly named indoor computer or indoor PC (personal computer).

Several parameters are computed from measurements taken by the Sensor Unit, including rainfall rate, drop size distribution (DSD) and oblateness. Other measured parameters are compared with calculations from well-known models.

To begin with, consider rainfall rates. These are not based in time as one would expect, but in quantity of rain in a given amount of time. The amount of rainfall rate displayed will be the rain accumulation for the last 30 minutes since the last 0.1 mm increment.

Another parameter displayed by VIEW_HYD is the DSD. It is calculated using

$$N(D_i) = \frac{1}{\Delta t \Delta D} \sum_{j=1}^{M_i} \frac{1}{A_j v_j} \left[\frac{1}{m^3 mm} \right] \qquad \textbf{3.1}$$

where Δt is the integration time interval in seconds, ΔD is the width of size class in mm, A_j is the effective measuring area of drop j in m^2, v_j is the velocity of drop j in $m \cdot s^{-1}$, I is the drop size class, j is the single drop, M_i is the number of drops in class I during Δt, and D_i is the diameter of class i.

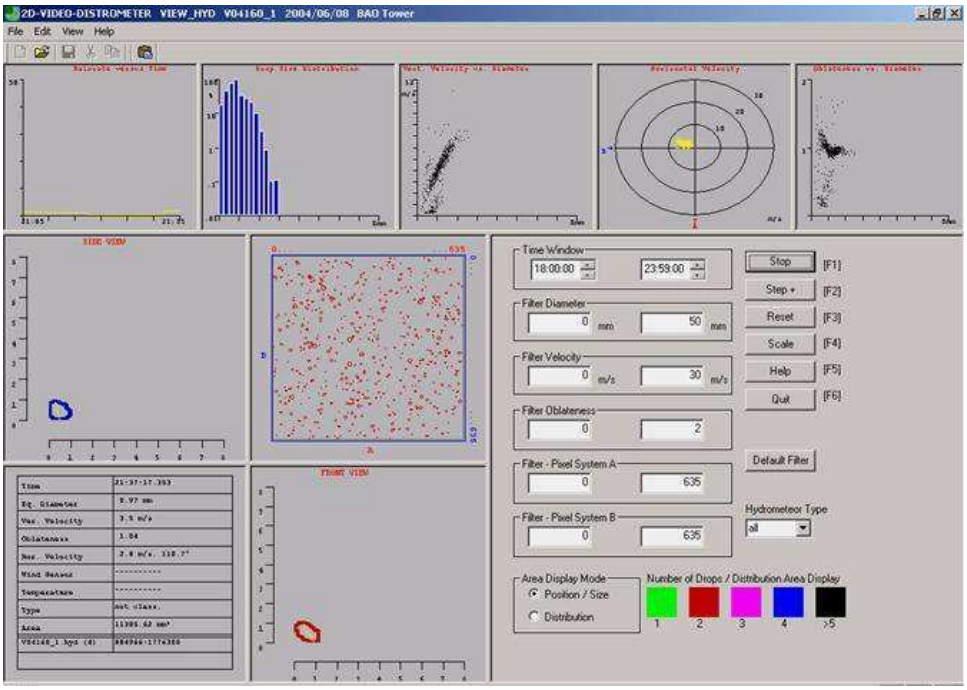

Figure 3-4. Image of the VIEW_HYD software that provides rainfall and raindrops information.

Regarding vertical velocity, as stated before, is measured by the difference in distance between light planes, but it also is compared with computed velocity determined after *Atlas* et al. (1973). This relation is given by

$$v(D) = 9.65 - 10.3e^{-0.6D} \qquad \textbf{3.2}$$

where v is the velocity in $m \cdot s^{-1}$ and D is the diameter in mm.

Every 3 seconds, data are "packaged" by the OEU PC and transmitted via TCP/IP to the Indoor User Terminal, a third component that is described below.

4 Data Sets

4.1 Comparison between 2DVD, rain gauges and TRMM data

4.1.1 TRMM Location Computation

In order to compare 2DVD data with the one from TRMM, an area over the 2DVD's position is needed to take data from TRMM. By using the circular orbit attitude (r = 350 km, TRMM θ=0.25 degrees) approximating to a triangle, as in (4.1), the edges of the triangle is calculated, which defines the area to be taken from TRMM, as it can be seen in Figure 4-1.

$$s = r\tan(\theta) \qquad \textbf{4.1}$$

Notice that s values are typically given in km, but localization data in TRMM's website is available in degrees, so conversion between them is required. Using that value in degrees and knowing 2DVD's position (latitude = 18.26, longitude = -66.00), the area where data should be taken is then easily obtained, as shown in Figure 4-1.

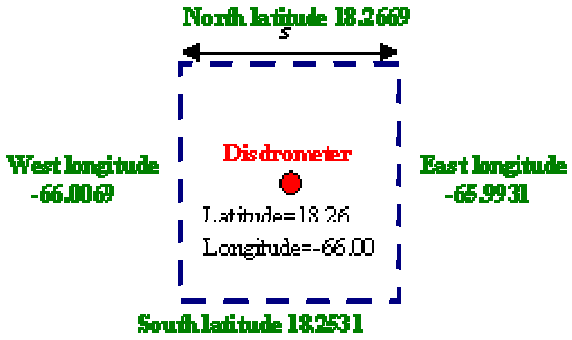

Figure 4-1. Disdrometer position and area to be taken from TRMM

4.1.2 Data Comparison per Hour

The comparison took place with data collected from September 15th to 16th, 2004, dates in which the tropical storm Jeanne passed over Puerto Rico. The root-mean-squared (RMS) error was computed for each case.

Since the TRMM data from NASA TOVAS is provided every 3 hours and 2DVD is obtained every minute, we computed the rain rate per hour for 2DVD data and average rain rate per hour for TRMM data.

To co-locate in time (local AST time), 4 hours were subtracted from the original 2DVD data, which is given in UT. NCDC rain gauges, measured in inches, were changed to millimeters, before comparing it to disdrometer data.

Cumulative rain rate was also computed for each day, for each sensor.

4.2 Characterizing Puerto Rico's rain and rain rate estimate algorithm evaluation

4.2.1 Flow diagram

The flow diagram showed in Figure 4-2 describes all the steps that were required in order to compute coefficients for every estimator from the raw data files produced by the 2DVD.

The 2DVD generates proprietary files (with HYD extension) containing rainfall data. These files are converted into text-files by using an external program called FIRM_DSD to ease the data manipulation afterwards.

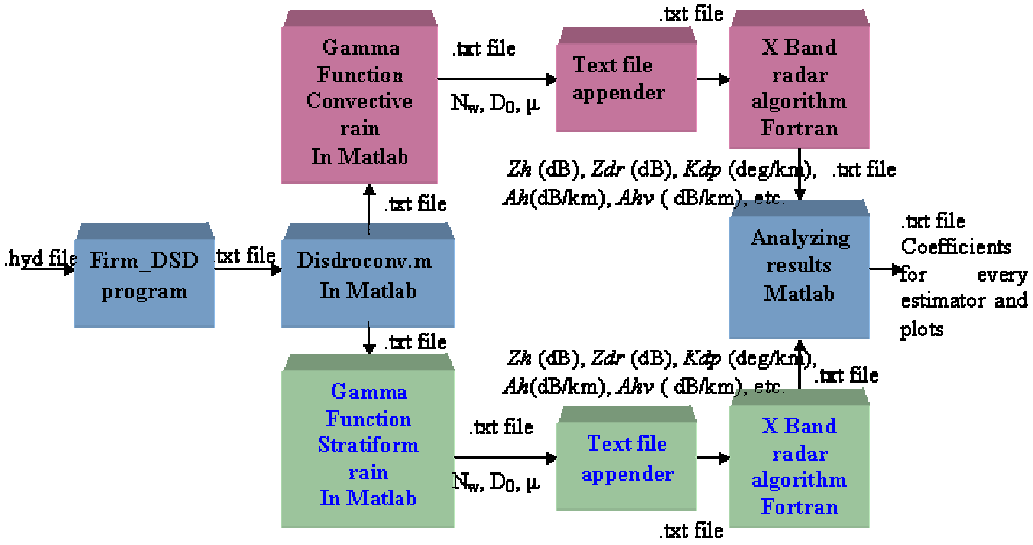

Figure 4-2. Flow diagram for the rainfall data manipulation, calculations, analysis and result generation process.

CSU developed Matlab codes in charge of stratiform/convective data classification as well as computing additional gamma function parameters. This code, implemented by Dr. Huang, and provided by Dr. Bringi, requires an input text-file that Matlab can automatically load. Since the text-files generated by FIRM_DSD contain non-desired characters, another Matlab code was written in order to clean them up. This code is referred to in this project as Disdroconv.m.

The set of files outputted by the gamma function Matlab codes contain, along other information, the gamma function parameters. These sets of files were, then, unified into a single file by using the Text-file appender software implemented for this purpose. By handling one file instead of dozens, significant data processing time was saved from the remaining steps in the process.

CSU also provided second application software, enabling the simulation of X-Band polarimetric radar static shape of drops and drop oscillations. With the unified file produced by the text-file appender, this FORTRAN application outputs the radar parameters through another text-file that Matlab can load for later analysis and plots generation.

4.2.2 FIRM_DSD

Rainfall collection during the day will be computed by using a C-language program called FIRM_DSD. This program converts proprietary .hyd files to a text file that can be used later to analyze the data. The resulting text file provides DSD information and rain-rate, integrated by the amount of seconds chosen by the user. Table 4-1 presents a portion of a text file generated with the FIRM_DSD.

Table 4-1. Portion of text file generated using FIRM_DSD program. Note that the last line shows rain-rate for the time period presented.

Time			**Radius range**				**N(D)**		
7:00:00	->	7:01:00	0	->	0.25	mm	n=	2834.141	/m3mm
7:00:00	->	7:01:00	0.25	->	0.5	mm	n=	10352.36	/m3mm
7:00:00	->	7:01:00	0.5	->	0.75	mm	n=	8125.599	/m3mm
7:00:00	->	7:01:00	0.75	->	1	mm	n=	9398.197	/m3mm
7:00:00	->	7:01:00	1	->	1.25	mm	n=	10177.08	/m3mm
7:00:00	->	7:01:00	1.25	->	1.5	mm	n=	3756.905	/m3mm
7:00:00	->	7:01:00	1.5	->	1.75	mm	n=	1055.946	/m3mm
7:00:00	->	7:01:00	1.75	->	2	mm	n=	370.7528	/m3mm
7:00:00	->	7:01:00	2	->	2.25	mm	n=	202.2668	/m3mm
7:00:00	->	7:01:00	2.25	->	2.5	mm	n=	138.3082	/m3mm
7:00:00	->	7:01:00	2.5	->	2.75	mm	n=	86.90639	/m3mm
7:00:00	->	7:01:00	2.75	->	3	mm	n=	29.29995	/m3mm
7:00:00	->	7:01:00	3	->	3.25	mm	n=	14.46472	/m3mm
7:00:00	->	7:01:00	3.25	->	3.5	mm	n=	2.659475	/m3mm
7:00:00	->	7:01:00	3.5	->	3.75	mm	n=	2.591645	/m3mm
7:00:00	->	7:01:00	3.75	->	4	mm	n=	1.512695	/m3mm
rain-rate	=							42.50055	mm/hr

4.2.3 Classifying rain type

There are two methods for classifying rain type; this study used both of them because they are useful in order to compare with other studies in different geographical regions. For characterizing Puerto Rico rainfall the method used was the second one.

4.2.3.1 First method

Maki et al. found an empirical line for classifying the rain in convective or stratiform as shown in Figure 4-3. The points up the line are classified as convective and down the line as stratiform.

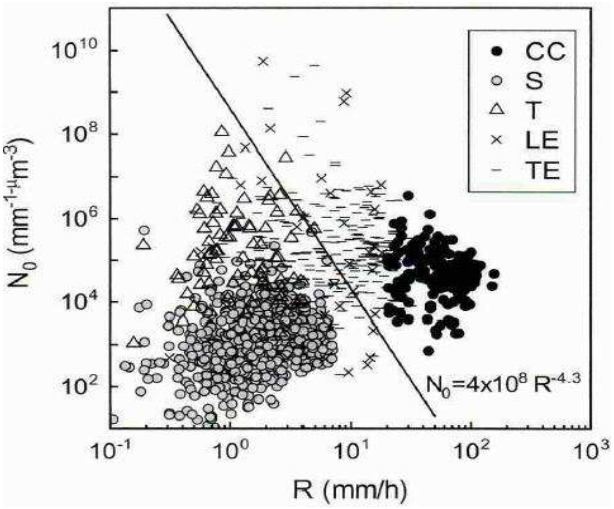

Figure 4-3 The N_0-R scatter plot. The line $N_0=4 \times 10^8 R^{-4.3}$ shown is the empirical convective-stratiform rainfall classification line, *Maki* et al 2001.

4.2.3.2 Second method

The criteria used to distinguish between convective and stratiform rain is typically defined as $R > 0.5$ mm/hr with a standard deviation of $R < 1.5$ mm/hr for the latter, whereas convective rain requires $R > 5$ mm/hr with a standard deviation of $R > 1.5$ mm/hr.

4.2.4 Text file appender

After having identified that the data manipulation process was the same for each input file, since it is independent of the time-range included in those files, the need of appending all the available input files into one was evident. That would save the time spent in several iterations of this process. With that motivation in mind, an application able to append any set of text-files in a specified order was implemented.

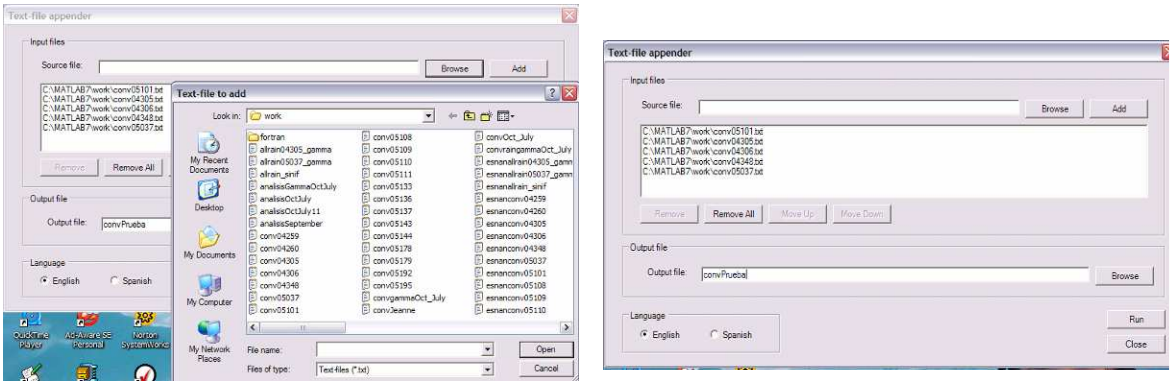

(a) **(b)**

Figure 4-4. Text file appender program (a) Selecting multiple files (b) Assigning a file order and output file name.

The text-file appender is a Windows-based application that addresses this need in a two-step process. First, it allows selecting multiple files and specifying the order in which those files will be appended with each other. This step can be seen in Figure 4-4(a). Secondly, the output filename needs to be entered prior to running the operation, as it can be depicted in Figure 4-4(b).

4.2.5 X-band radar algorithm

CSU developed a FORTRAN application enabling the simulation of X-Band polarimetric radar for static shape of drops and drop oscillations. Such a simulation will then be performed to examine the expected response in the upcoming CASA radar

network tested on the island. This simulation will provide the following polarimetric radar parameters: Z_H (dB), Z_{DR} (dB), K_{DP} (degree/km), A_H(specific attenuation, dB/km), A_{HV} (dB/km), r_{HV} (zero-copolar cross-correlation coefficient, no unit), del_{HV} (backscattering differential phase shift, degree), L_{DR} (linear depolarization ratio dB) and rainrate (mm/hr).

This algorithm was written by Dr. Chengxian Tang at the Radar Lab, Department of Electrical Engineering, Colorado State University. This is a fast and accurate multiparameter polarimetric radar model simulator for model precipitation of arbitrary cloud microphysics, written in FORTRAN-77. This code is initially developed to, but not limited to, be incorporated with the CSU-RAMS model to study the polarimetric radar observable structures during the cloud and precipitation evolution to give better understanding and estimation of cloud microphysics by making use of multiparameter polarimetric radars.

The algorithm is consisted of the following relatively independent packages.

The first package is the **ensemble estimation** package that adds up the incoherent contributions of all the scatterers within the radar range gate, by performing integrations over hydrometeor types, drop size distributions, drop canting angle distributions, and so on.

The second package is the **hydrometeor model** package that specifies the microphysical properties of single hydrometeors.

The third package is the **scattering computation** package for rotationally and equatorially symmetric dielectric particles.

There are sub-packages described as:

- T-matrix Method sub-package for general particles, and is coded basically based on the algorithm well developed and documented by Barber, P. and C. Yeh 1975. Distinguished from other T-matrix codes, this package directly recurs the ratios and products of Bessel functions instead of basic Bessel functions to avoid numerical errors that often occur when the argument and/or order of Bessel functions are large. Numerical implementation is carefully coded to reach the maximum computational speed and accuracy.
- Rayleigh Approximation sub-package for particles small compared with wavelength.
- Mie Solution sub-package for spherical particles, including routine.

All integrals are computed with the Gaussian-Legendre quadrature algorithm.

4.2.6 Estimation Methods

4.2.6.1 Classic estimation method of rain rate and rain water content

The direct fitting of the functional form $R=cZ_H^b$ may be not appropriate method because the range of Z_H is from 10^0 to 10^6 (mm^6m^{-3}), while R is from 0 to 10^2. *Maki* and *Bringi* (2005) confirmed that the functional form $log\ R=b\ logZ_H + logc$ gives more representative fitting results than did direct fitting. Thus, we calculated the coefficients b and c (b' and c') of the relationship $R=cZ_H^b$ ($M=c'Z_H^{b'}$) of the relation after taking logarithms of these relations.

4.2.6.2 Estimation of rain rate and rain water content with polarimetric variables.

Different combinations of polarimetric variables are possible for constructing rain rate estimators. The obtained regression fits for the R-K_{DP} relation for convective rain, stratiform rain and all rain type were using the direct fitting of the functional form $R(K_{DP}) = c_1 K_{DP}^{b_1}$ relationship, because for X-Band radar the range for K_{DP} is from 0 to 15 ˚km-1 [*Maki* and *Bringi*, 2005].

It is possible to construct rain estimators using a combination of polarimetric variables such as $R(K_{DP}, Z_{DR})$ and $R(Z_H, Z_{DR})$. For estimators of rain water content using polarimetric variables were applied similar to those for rain rate estimators.

5 Analysis and Results

5.1 Comparison between 2DVD, rain gauges and TRMM data

5.1.1 Data Comparison per Hour

With the goal of comparing 2DVD data with each one of the other devices (TRMM and NCDC), separate analyses were made, comparing TRMM against 2DVD and NCDC against 2DVD.

5.1.1.1 Hourly Data comparison Disdrometer-TRMM

Notice that TRMM data tends to overestimate the rain rate, as it can be seen in Figure 5-1(a); this is probably due to the averaging of areas where the rain was stronger, whereas the disdrometer was measuring only at one point, but in both days the RMS error was small.

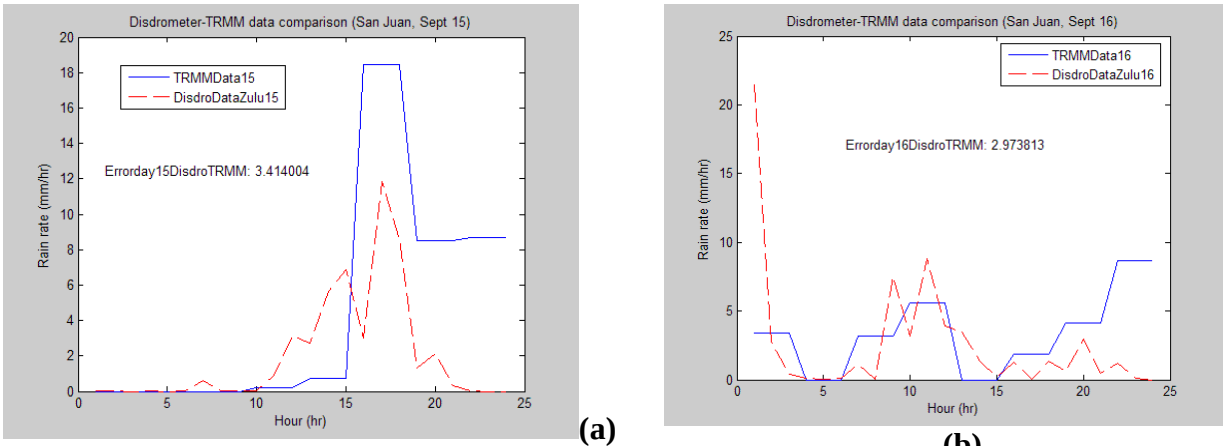

(a) **(b)**

Figure 5-1. Disdrometer-TRMM data comparison in San Juan for (a) Sept 15th and (b) Sept 16th 2004.

5.1.1.2 Hourly Data comparison Disdrometer-NCDC

To co-locate in time (local AST time), 4 hours were subtracted from the original 2DVD data, which is given in UT. NCDC rain gauges, measured in inches, were changed to millimeters, before comparing it to disdrometer data. As shown in Figure 5-2, disdrometer and rain gauge data compares very well. The RMS error comparing NCDC against 2DVD was significantly smaller than comparing against TRMM, which reveals a greater similarity between NCDC and 2DVD data than for TRMM.

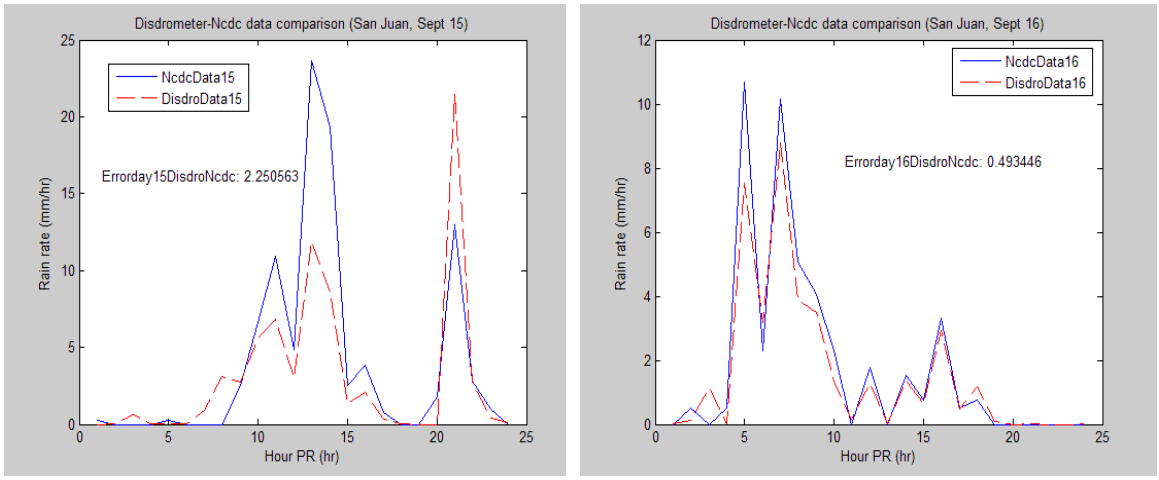

(a) **(b)**

Figure 5-2. Disdrometer-NCDC data comparison in San Juan for (a) Sept 15th and (b) Sept 16th 2004.

5.1.2 Cumulative data comparison

Cumulative rain rate was also computed for each day, for each sensor, as shown in Figure 5-3.

During the storm on Sept 15th, 2004 the disdrometer shows about half the accumulated rainfall than both, the rain gauge and the TRMM estimate.

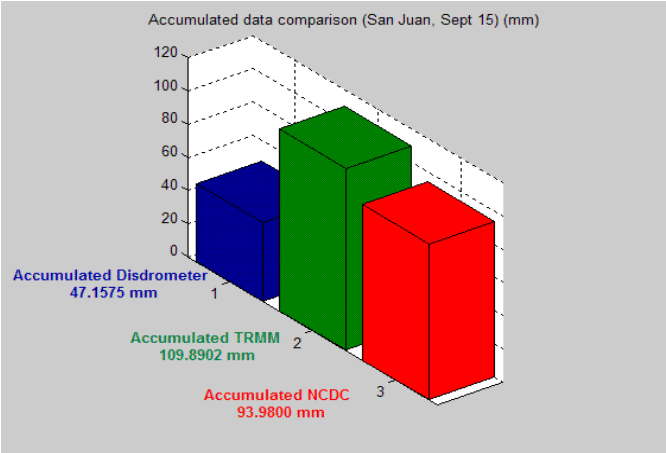

Figure 5-3. Disdrometer-TRMM-NCDC cumulative data comparison (San Juan, Sept 15, 2004).

Another rain gauge utilized for comparison purposes was one maintained by the National Weather Service (NWS), located very close to the 2DVD. Figure 5-4 compares such rain gauge against the other devices for Sept 16th. This data was not available for the 15th.

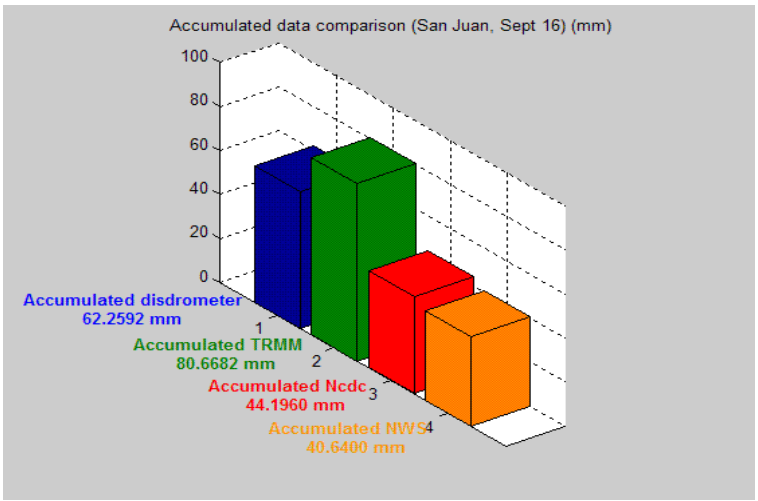

Figure 5-4. Disdrometer-TRMM-NCDC-Rain gauge NWS cumulative data comparison (San Juan, Sept 16, 2004).

5.2 Characterizing Puerto Rico's rain and rain rate estimate algorithm evaluation

5.2.1 October 2004 -July 2005

In order to characterize Puerto Rico rain, the first method proposed by Maki et al for classifying rain type was used. Figure 5-5 shows how was done it from October 2004 to July 2005. The points up the line are classified as convective and down the line as stratiform. 1519 are classified as stratiform and 776 as convective in total there are 2295 samples.

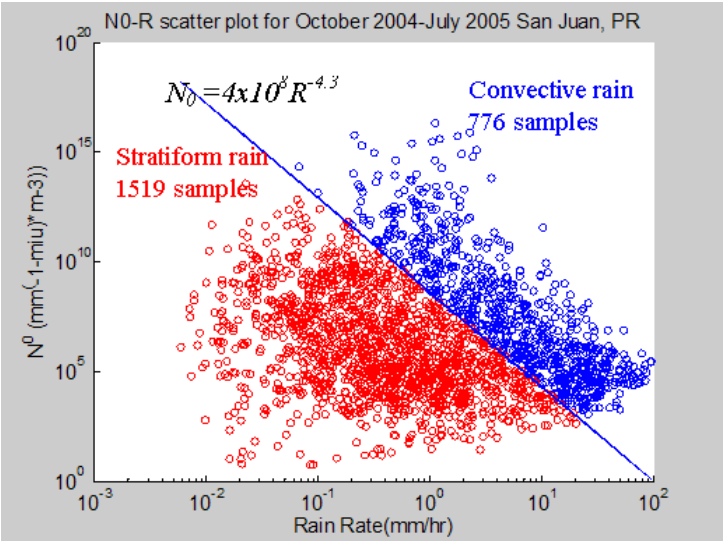

Figure 5-5. N_0-R scatter plot from October 2004 to July 2005.

Figure 5-6 shows how Drop Size Distribution from October 2004 to July 2005 is.

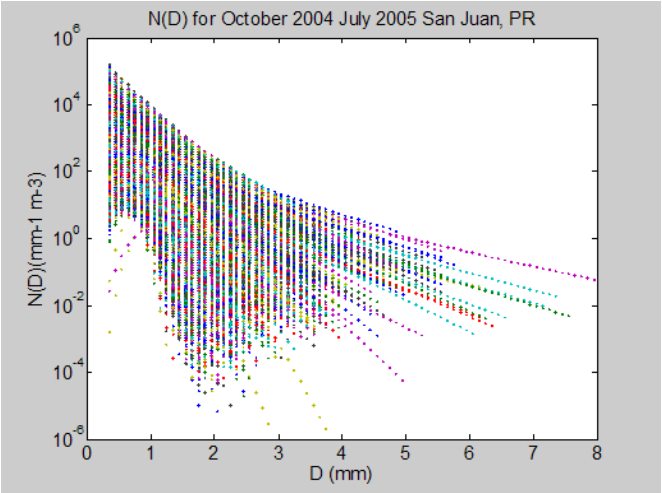

Figure 5-6.Drop size distribution using gamma function from October 2004 to July 2005.

5.2.1.1 Classic estimator by rain type classification

Scatter plot of R-Z_H and M-Z_H relations are shown in Figure 5-7(a) and Figure 5-7(b), respectively, for convective and stratiform rain R and M each point are calculated directly from two minute-averaged DSD while Z_H is calculated in Fortran algorithm provided by CSU, by the T-matrix method.

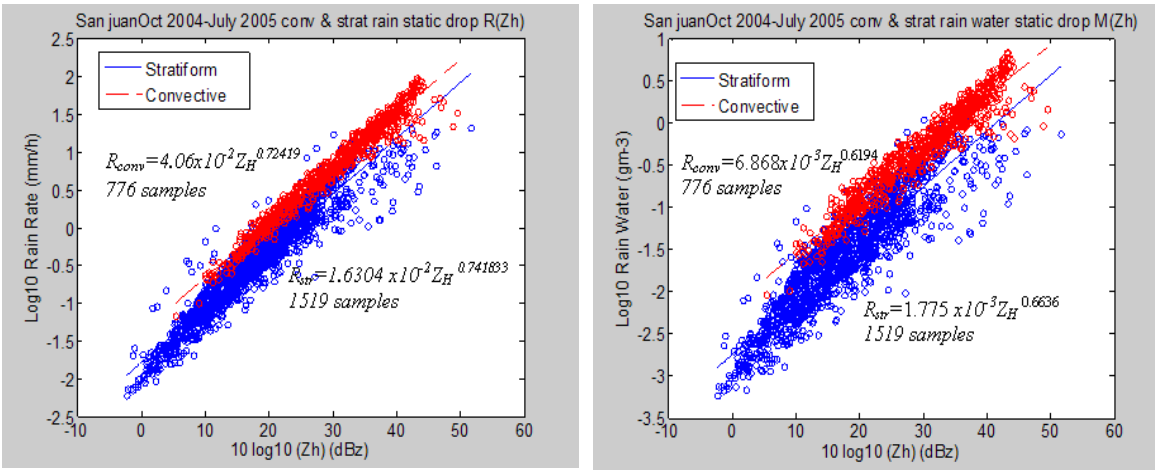

(a) **(b)**

Figure 5-7 Scatter plots of the reflectivity factor Z_H (a) and the rain rate R., and (b) and the rain water content M. Rain type is classified as stratiform (*str*) and convective (*conv*) using the threshold relation $N_0=4\ x10^8R^{-4.3}$ derived by *Maki* et al. (2001).

Z_h depends approximately on the 6th moment of DSD while R depends on the 3.6th moment; it's the principal reason for the variability in Figure 5-7(a). Additionally in the Figure 5-7(b) has the same variability but in this case M depends on the 3rd moment of DSD. The results of the least-square regression analysis are shown in Table 5-1and Table 5-2.

Table 5-1. Coefficients of the $R(Z_H) = cZ_H^b$ rainfall algorithm at X-band wavelength derived from disdrometer data collected during October 2004-July2005 in San Juan, Puerto Rico. R[mmh^{-1}] and Z_H [mm^{6}m^{-3}]. The form $log\ R = b log Z_H + log c$ was used to obtain $R = cZ_H^b$ relationship.

Rain Type	***c***	***b***
Convective	4.06 x10^{-2}	0.72419
Stratiform	1.6304 x10^{-2}	0.74183
All	**1.421x10^{-2}**	**0.82158**

Table 5-2.Same as in the Table 5-1, but for $M(Z_H) = c'Z_H^{b'}$, where M [gm^{-3}], and Z_H [mm^{6}m^{-3}]. The form log $R=b'$logZ_H + logc' was used to obtain $M = c'Z_H^{b'}$ relationship.

Rain Type	***c'***	***b'***
Convective	6.868 x10^{-3}	0.619424
Stratiform	1.775 x10^{-3}	0.663642
All	**1.516 x10^{-3}**	**0.764582**

This analysis does not included error factors as effect of attenuation, radar calibration errors, beam blockage, instrumental noise, etc.

5.2.1.2 Rain rate and rain water content with polarimetric variables

Different combinations of polarimetric variables are possible for constructing rain rate estimators. The obtained regression fits for the R-K_{DP} relation for convective rain, stratiform rain and all rain type were using the direct fitting of the functional form $R(K_{DP}) = c_1 K_{DP}^{b_1}$ relationship, because for X-Band radar the range for K_{DP} is from 0 to

15 °km^{-1}. In order to analyze the variations in DSD, it is important to study the dispersion of plotted samples in the R-K_{DP} diagram Figure 5-8(a) and in the R-Z_H diagram in Figure 5-7(a), concluding that the variations in R-K_{DP} are smaller than in the estimator R-Z_H.

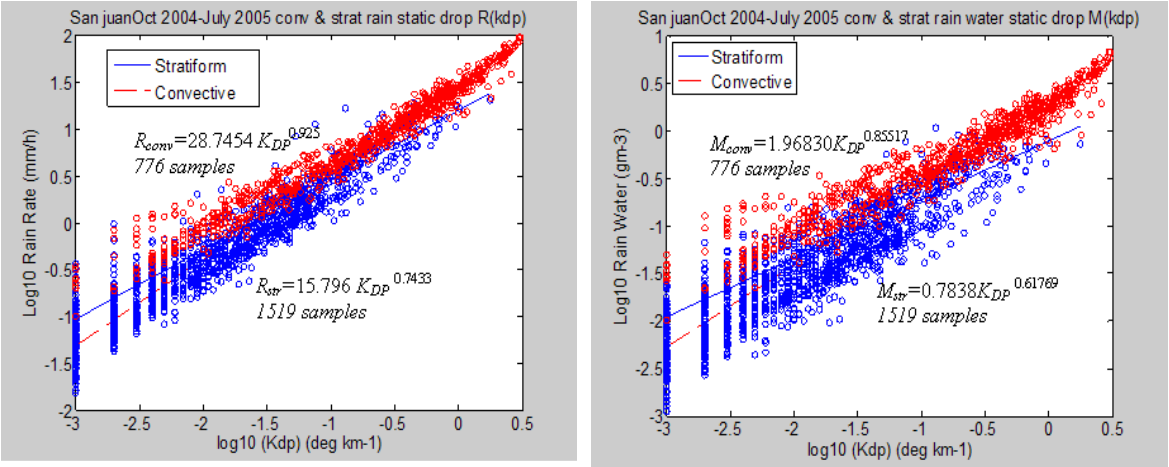

(a) **(b)**

Figure 5-8. Scatter plot of the specific differential phase K_{DP} (a) and the rain rate R, and (b) and the rain water content M. Rain type is classified as stratiform (*str*) and convective (*conv*) using the threshold relation $N_0=4\ x10^8R^{-4.3}$ derived by *Maki* et al. (2001).

Table 5-3. Coefficients of the $R(K_{DP}) = c_1 K_{DP}^{b_1}$ rainfall algorithm at X-band wavelength derived from disdrometer data collected during October 2004-July2005 in San Juan, Puerto Rico. R ≥ 1 mmh^{-1}. R[mmh^{-1}] and K_{DP} [deg km^{-1}].

Rain Type	c_1	b_1
Convective	28.7454	0.925
Stratiform	15.796	0.7433
All	**27.8856**	**0.9593**

Table 5-4. Coefficients of the $M(K_{DP}) = c_1 K_{DP}^{b_1}$ rainfall algorithm at X-band wavelength derived from disdrometer data collected during October 2004-July2005 in San Juan, Puerto Rico. R ≥ 1 mmh^{-1}. M [gm^{-3}] and K_{DP} [deg km^{-1}].

Rain Type	c_1	b_1
Convective	1.96830	0.85517
Stratiform	0.7838	0.61769
All	**1.87898**	**0.91228**

Table 5-5. Same as in Table 5-3 except for $R(Z_H, Z_{DR}) = c_3 Z_H^{a_3} 10^{0.1 b_3 Z_{DR}}$, where R[mmh^{-1}], Z_H[mm^{6}m^{-3}], and Z_{DR} [dB].

Rain Type	c_3	a_3	b_3
Convective	2.3363x 10^{-2}	0.85547	-3.64682
Stratiform	1.2101x 10^{-2}	0.93832	-5.26388
All	**1.1692x 10^{-2}**	**0.96966**	**-5.6958**

Table5-6. Same as in Table 5-4 except for $M(Z_H, Z_{DR}) = c_3 Z_H^{a_3} 10^{0.1 b_3 Z_{DR}}$, where M [gm^{-3}], Z_H[mm^{6}m^{-3}], and Z_{DR} [dB].

Rain Type	c_3	a_3	b_3
Convective	3.482 x 10^{-3}	0.78065	-4.47855
Stratiform	1.215 x10^{-3}	0.91311	-6.68311
All	**1.178 x 10^{-3}**	**0.95626**	**-7.37265**

5.2.1.3 Comparing results with other locations and estimators

The coefficients found for the relationship $R(Z_H)$ in Puerto Rico are between the coefficients found by Marshall and Palmer and used by NEXRad, as show in Figure 5-9.

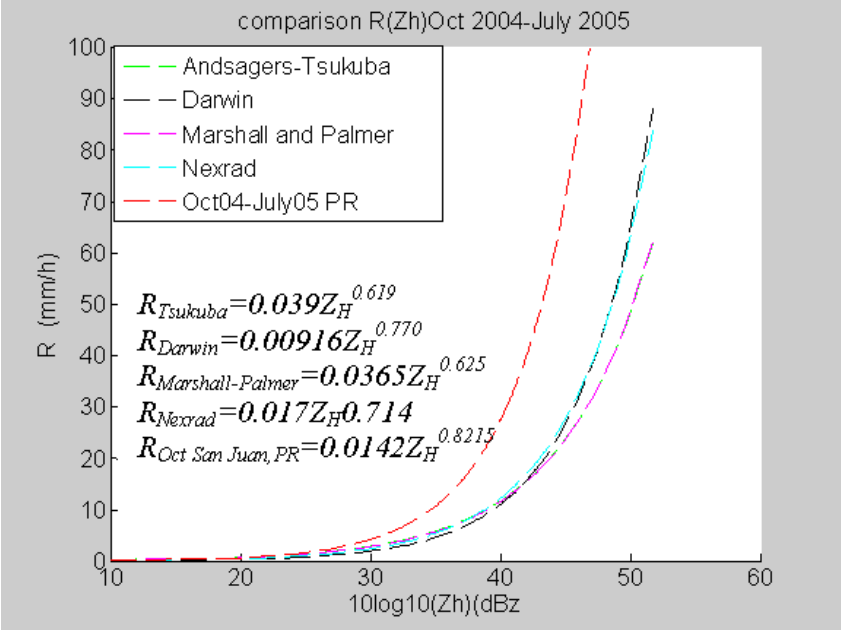

Figure 5-9. The dependence of rain estimator R-Z_H on geographical location or for different axis ratio formulae.

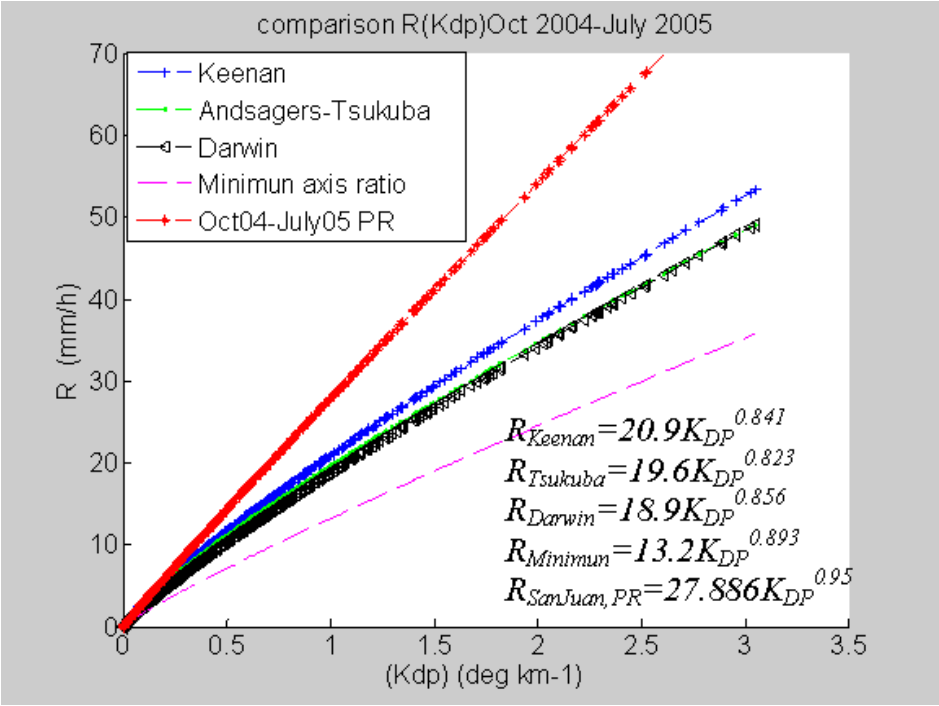

Figure 5-10. The dependence of rain estimator R-K_{DP} on geographical location or for different axis ratio formulae.

5.2.1.4 Estimation error due to DSD variations

Figure 5-11(a, b and c) show comparisons of rain rates R computed for estimators $R(Z_H)$, $R(K_{DP})$ and $R(Z_H, Z_{DR})$ with rain rates R_{dis} calculated from observed raindrop size spectra. From this scatter plots, it can be suggested that the worst estimator of the three is $R(Z_H)$, which is most sensitive to variations in DSD and tend to overestimate rain. On the other hand, the tendency points to $R(K_{DP})$ as the most accurate estimator from the point of view of the insensitiveness to variations in DSD.

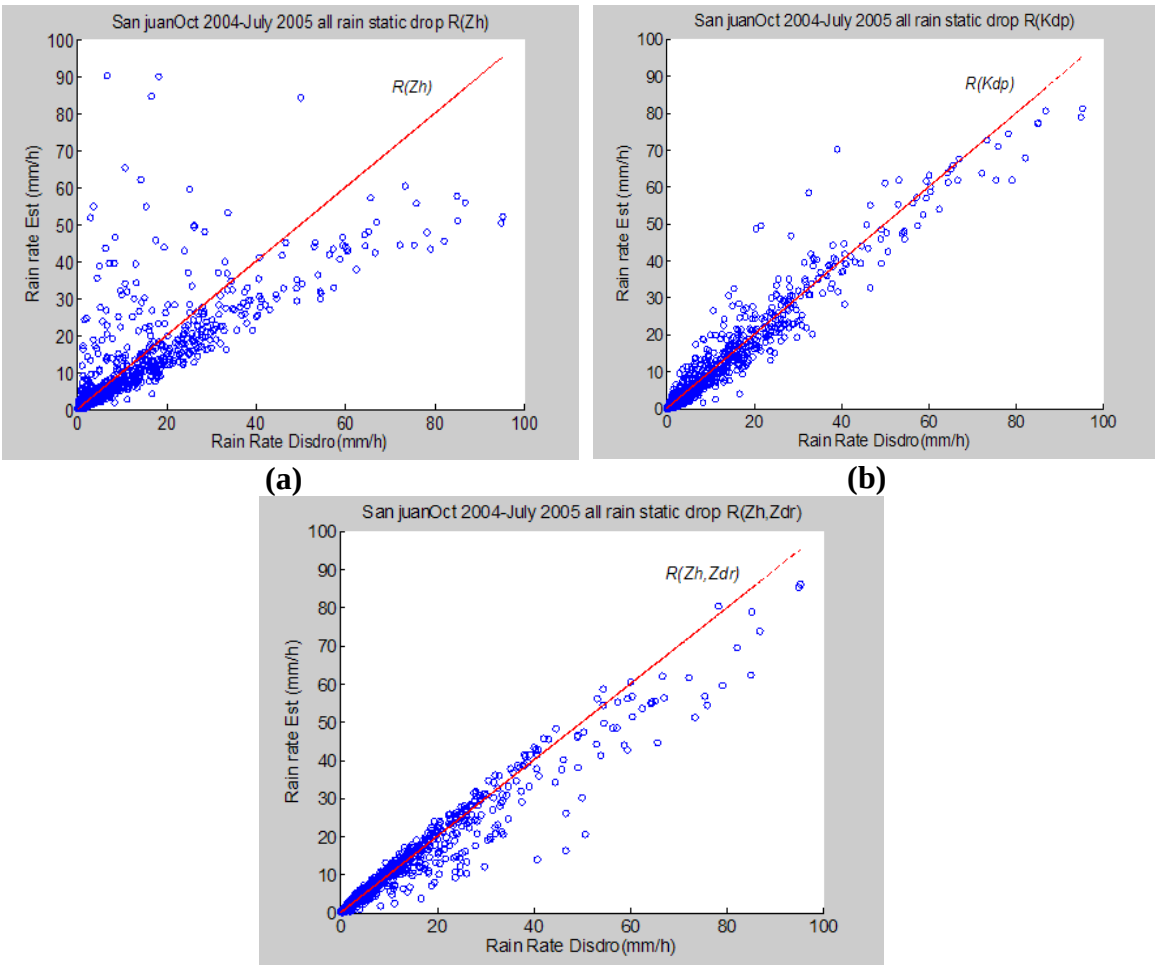

Figure 5-11.Scatter plots of R_{dis} calculated from measured drop size distribution and R estimated by (a) $R(Z_H)$, (b) $R(K_{DP})$, (c) $R(Z_H, Z_{DR})$.

Figure 5-12(a, b and c) show comparisons of rain water content M computed for estimators $M(Z_H)$, $M(K_{DP})$ and $M(Z_H, Z_{DR})$ with rain water content M_{dis} calculated from observed raindrop size spectra. These scatter plots also suggest that the worst estimator of the three is $M(Z_H)$, while $M(K_{DP})$ tends to be the most accurate from the point of view of the insensitiveness to variations in DSD.

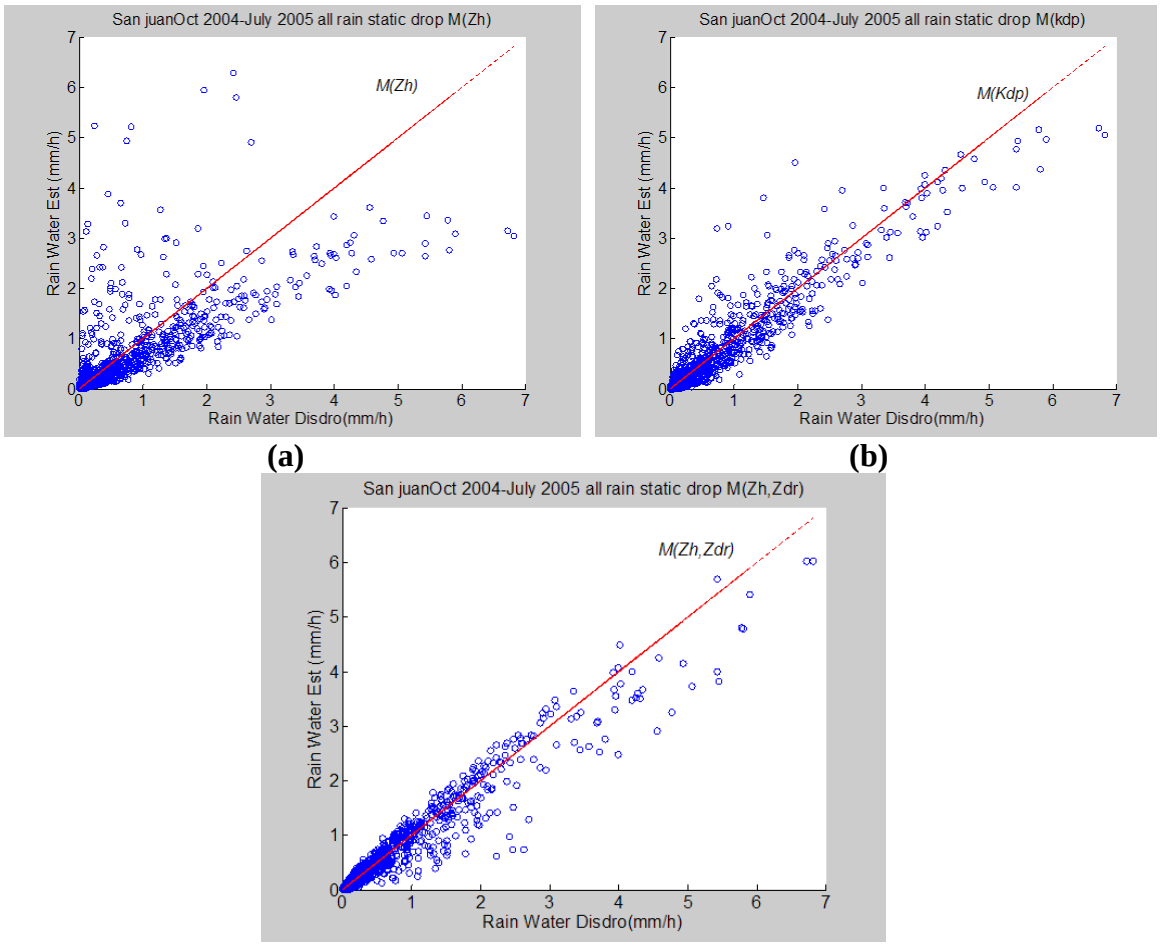

Figure 5-12. Scatter plots of M_{dis} calculated from measured drop size distribution and M estimated by (a) $M(Z_H)$, (b) $M(K_{DP})$, (c) $M(Z_H, Z_{DR})$.

The computed average NEs of $R(Z_H)$, $R(K_{DP})$ and $R(Z_H, Z_{DR})$ for all data samples were 40.86%, 14.73% and 15.83% respectively as it can be seen in Figure 5-13(a). The statistical errors for each estimator of rain water content M due to natural variations in DSD are shown in Figure 5-13(b). The $M(Z_H)$ estimator was clearly the most sensitive variations in the DSD, while the other three alternated as the least sensitive.

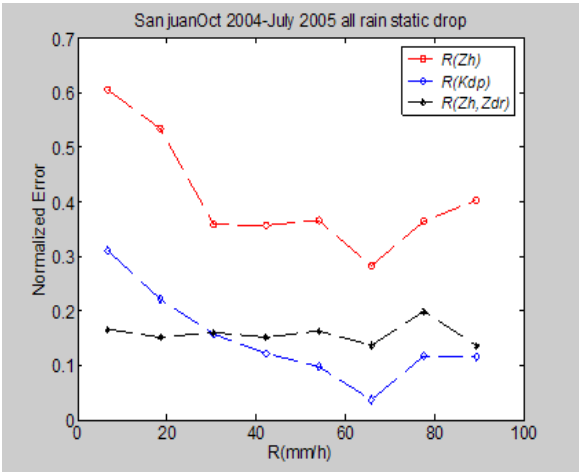

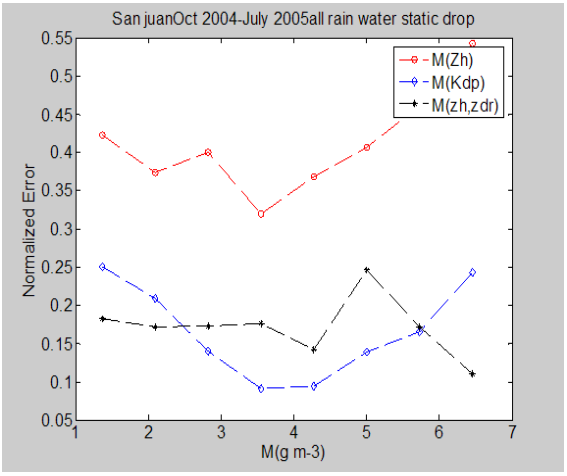

(a) **(b)**

Figure 5-13. Normalized error of three types of (a) rain rate estimators; $R(Z_H)$, $R(K_{DP})$ and $R(Z_H,Z_{DR})$, (b) rain water estimators; $M(Z_H)$, $M(K_{DP})$ and $M(Z_H,Z_{DR})$.

The average PRMSE of $R(Z_H)$, $R(K_{DP})$ and $R(Z_H, Z_{DR})$ for all data samples were 40%, 12%, and 18% respectively as it can be seen in Figure 5-14(a). The same statistical errors for each estimator of rain water content M due to natural variations in DSD are shown in Figure 5-14(b).

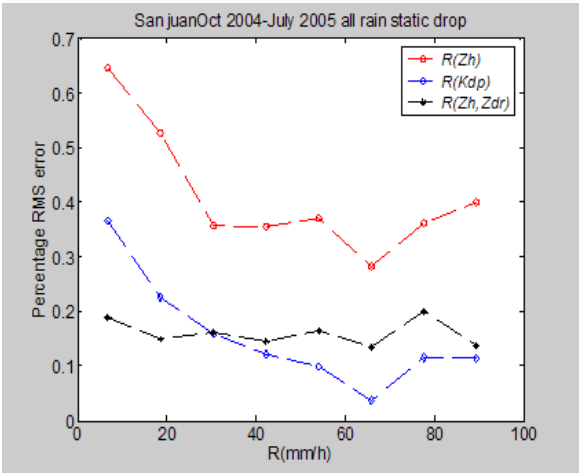

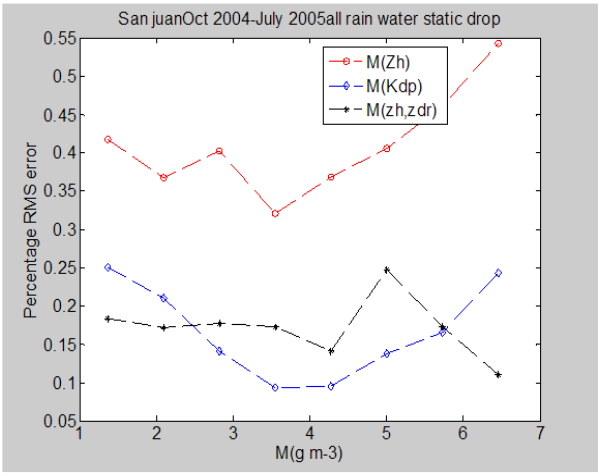

(a) **(b)**

Figure 5-14. Percentage RMS error of three types of (a) rain rate estimators; $R(Z_H)$, $R(K_{DP})$ and $R(Z_H,Z_{DR})$, (b) rain water estimators; $M(Z_H)$, $M(K_{DP})$ and $M(Z_H,Z_{DR})$.

Figure 5-15(a) shows the MRE error of $R(Z_H)$, $R(K_{DP})$ and $R(Z_H, Z_{DR})$. Note that MRE tends to decrease with increasing rain rate. Figure 5-15(b) shows the MRE of the equivalent M estimators. MRE also tends to decrease with increasing rain rate. While the MRE of the classic estimator $R(Z_H)$ for rain rates larger than 10 mm/h is about 1600%, the MREs of polarimetric estimators $R(K_{DP})$ and $R(Z_H, Z_{DR})$ for the same rain rate intervals are 200%, and 90% respectively. From these comparisons, we can conclude that $R(K_{DP})$ is the least sensitive to variations in DSD.

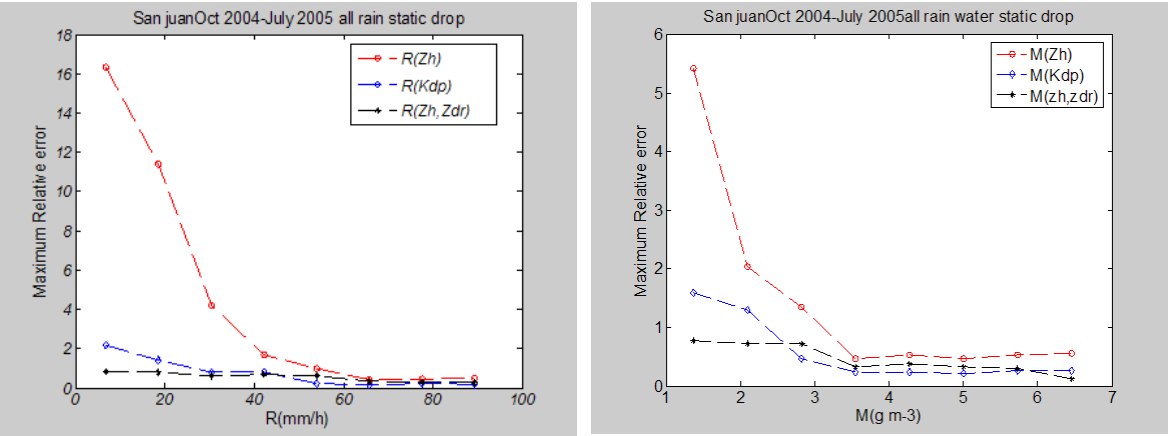

(a) **(b)**

Figure 5-15. Maximum relative error of three types of (a) rain rate estimators; $R(Z_H)$, $R(K_{DP})$, and $R(Z_H,Z_{DR})$, (b) rain water estimators; $M(Z_H)$, $M(K_{DP})$ and $M(Z_H,Z_{DR})$.

5.2.1.5 Effect of unusual DSD on polarimetric rain estimators

The R-K_{DP} method is less sensitive to variations in DSD, and there are several samples where R-K_{DP} method overestimated the rain rate. Figure 5-16 show relative errors of each DSD samples, where the values of R_{est}-R_{dis} greater than 20 mmh^{-1} are samples where rain rate is overestimated, these samples are called 'Unusual'.

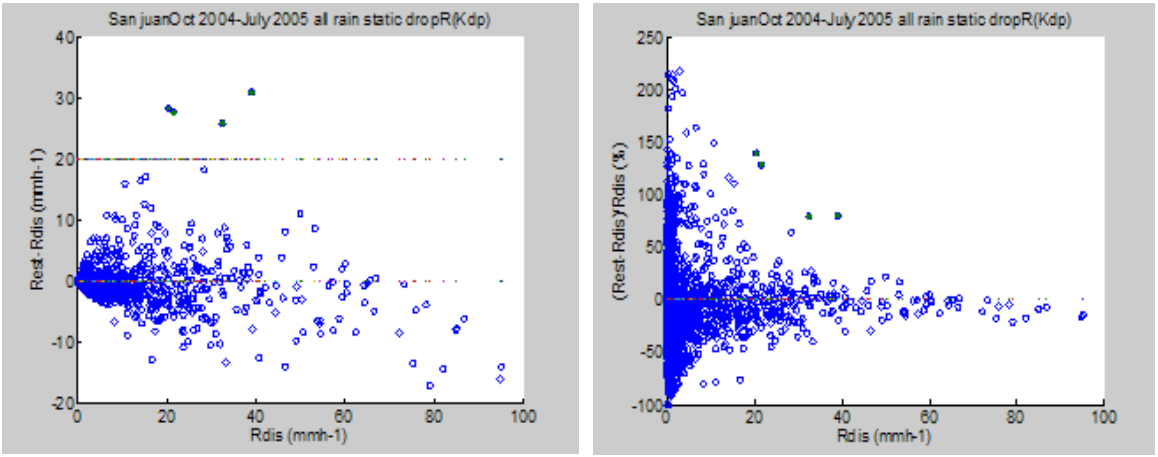

Figure 5-16. Relationship between relative error of $R(K_{DP})$ and R. Samples which have errors larger than about 20 mmh^{-1} are numbered.

To examine the more general error structure of polarimetric rain estimators, these parameters of the gamma DSD function, which rain rates were overestimated were compared with the statistical properties of all DSD samples. Histograms of gamma DSD parameters are summarized in Table 5-7. According to Figure 5-17, DSD parameters are widely distributed: the central percentiles of $\log_{10}(N_w)$, D_0, Λ, and μ are 0.4107~ 0.7189, 0.5767~1.3596, 2.0242~ 23.053, -1.5 ~ 11.

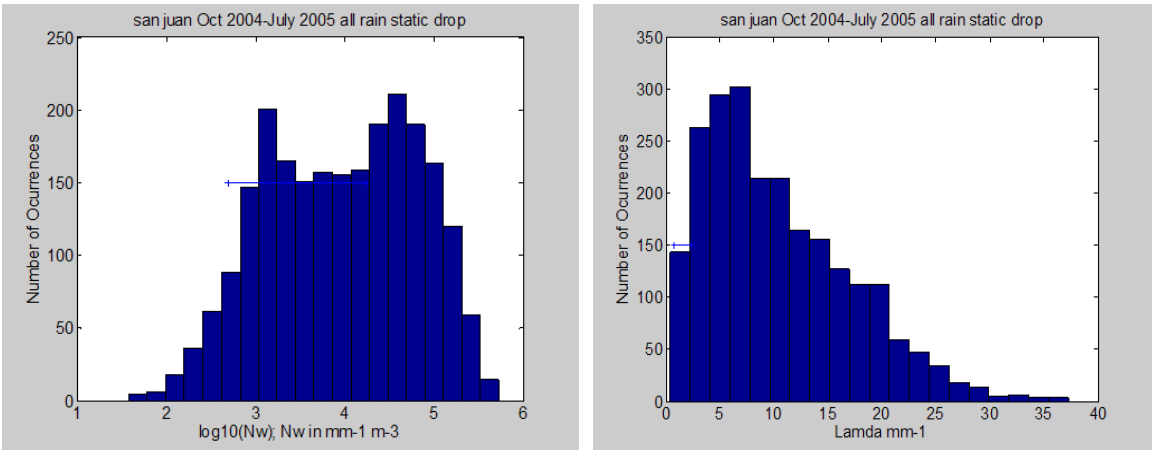

(a) **(b)**

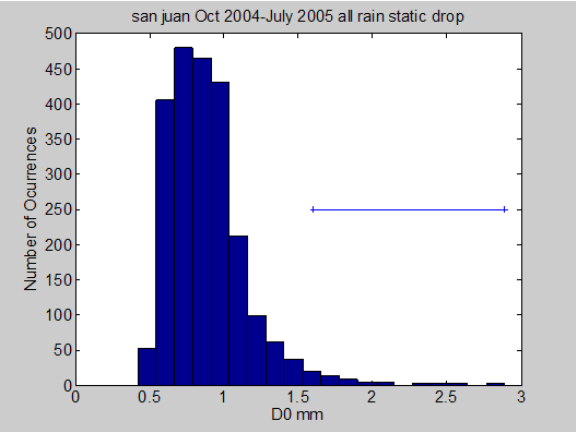

(c) **(d)**

Figure 5-17.Histogram of gamma DSD parameter (a) N_W, (b) Λ, (c) D_0, (d) μ of analyzed data. Arrows ranges of gamma DSD parameters for numbered samples in Figure 5-16.

Table 5-7 Summary of statistic of gamma DSD parameters for October 2004-July 2005 collected in San Juan, Puerto Rico.

	$\text{Log}_{10}(N_w)$ (m^{-3} mm^{-1})	D_0 (mm)	Λ (mm^{-1})	μ
Average value	4.5759	0.8837	10.4438	4.4255
Modal value	4.8	0.9	2.5	0
Standard deviation	4.7865	0.2640	6.7070	3.8946
Central 90 percentile	0.4107~ 0.7189	0.5767~1.3596	2.0242~ 23.053	-1.5 ~ 11

Figure 5-17 show with arrows the ranges of gamma DSD parameters of 'unusual' samples, that overestimation occurred when DSDs were characterized by small Λ values, or large D_0 values. The intercept parameter N_w for overestimated values is smaller than the modal value of all samples, as show in Table 5-7 and Table 5-8.

Table 5-8 Summary of statistic of gamma DSD parameters and polarimetric values for unusual samples during October 2004-July 2005 collected in San Juan, Puerto Rico.

Unusual sample	$\text{Log}_{10}(N_w)$ (m^{-3} mm^{-1})	D_0 (mm)	Λ (mm^{-1})	μ	Z_{HH}	Z_{DR}	K_{DP}	R
First	2.690543	2.887785	0.751441	-1.5	51.729	3.424	1.788	20.361965
Close_First					40.138	1.360	0.907	20.321000
Second	3.686960	1.932610	1.122834	-1.5	49.614	2.663	2.163	32.598896
Close_second					38.955	0.581	1.111	32.565025
Third	3.399219	2.115212	1.498668	-0.50	48.838	2.722	1.814	21.647363
Close_third					36.072	0.602	0.550	21.515875
Fourth	4.233831	1.603277	2.289062	0.0	47.006	1.944	2.611	39.012657
Close_Fourth					38.677	0.353	1.137	39.321596

Table 5-8 show the main characteristics of unusual samples, where $Log_{10}(N_w)$ for overestimated values is less than average value of all samples. Additionally Z_H, Z_{DR} and K_{DP} for values closer than unusual values are less than these values for unusual samples.

5.2.1.6 Further improvement in the accuracy of rain estimators using Z_{DR}

Unfortunately, of the three parameters, only D_0 can be directly related to Z_{DR} by a power law form as shown in Figure 5-18. This fact has been pointed out by several researches. *Seliga* and *Bringi* (1976) first showed that D_0 was a function of Z_{DR} when the DSD was exponential. *Bringi* et al. (1998) found a D_0-Z_{DR} relationship by analyzing DSD in thunderstorms using an airborne particle imaging sensor. *Maki* et al. (2005) found the flow relationship $D_0=1.59\ Z_{DR}^{0.447}$, in the present study for October 2004-July 2005 found the relationship $D_0 = 1.2559_{DR}^{0.3178}$ as show in Figure 5-18.

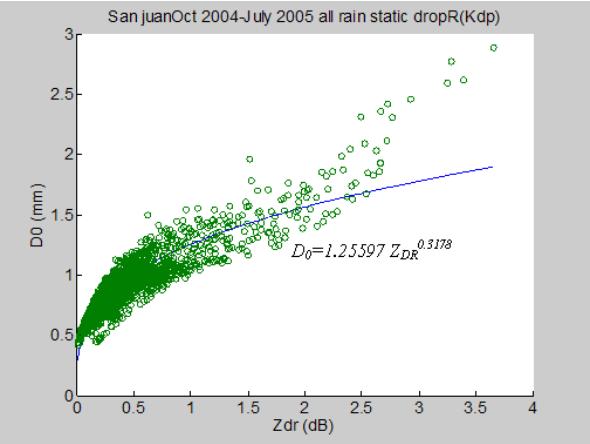

Figure 5-18. Relation between D_0 and Z_{DR}. The blue line shown is least square fitting curve.

5.2.1.7 Potential of X-band polarimetric radar for operations use

Figure 5-19 shows the dependence of the relationship between K_{DP} and R on the wavelength. According to Figure 5-19, the increase in sensitivity of K_{DP} is remarkable at the X-Band wavelength.

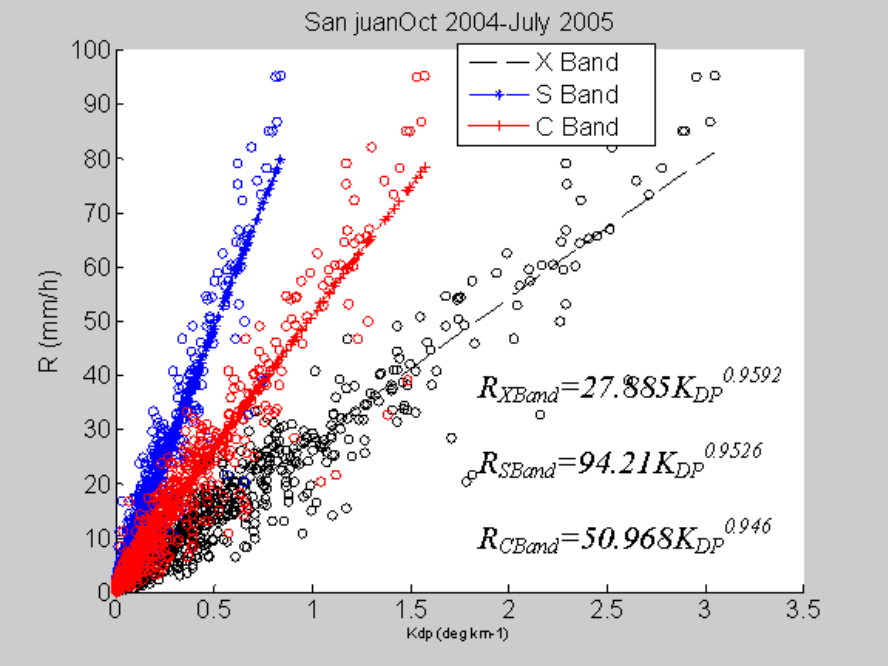

Figure 5-19. Dependence of R-KDP relations on wavelength.

5.2.2 September 15-16 2004 (Tropical Storm Jeanne)

In order to characterize Puerto Rico rain, the first method proposed by Maki et al for classifying rain type was used. Figure 5-20 shows how was done it for 15th and 16th September 2004. The points up the line are classified as convective and down the line as stratiform. 533 are classified as stratiform and 135 as convective in total there are 668 samples.

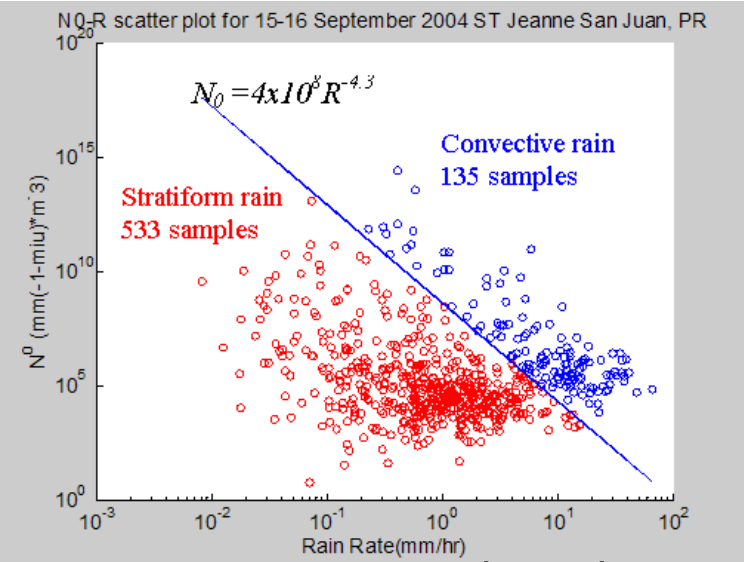

Figure 5-20.*N_0-R* scatter plot for 15th and 16th September 2004.

Figure 5-21 shows how Drop Size Distribution for 15th and 16th September 2004 is.

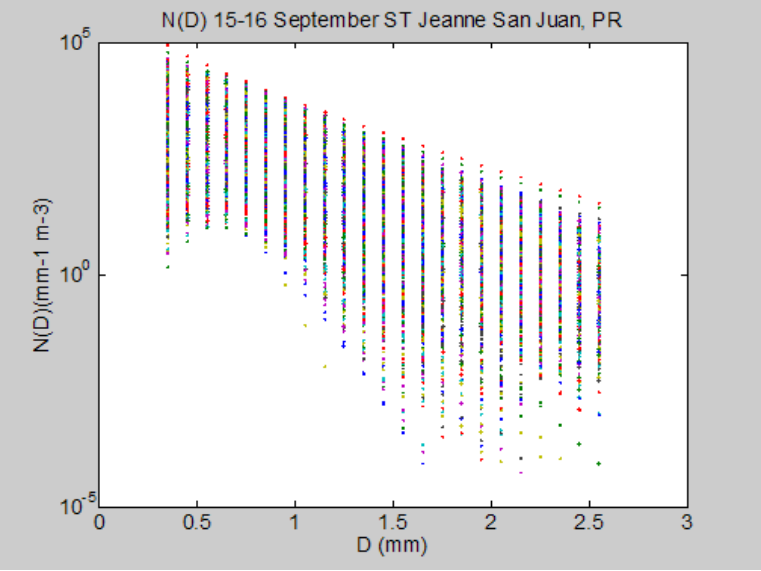

Figure 5-21. Drop size distribution using gamma function for 15th and 16th September 2004.

5.2.2.1 Classic estimator by rain type classification

Scatter plot of R-Z_H and M-Z_H relations are shown in Figure 5-22 for convective and stratiform rain R and M each point are calculated directly from two minute-averaged

DSD while Z_H is calculated in Fortran algorithm provided by CSU, by the T-matrix method.

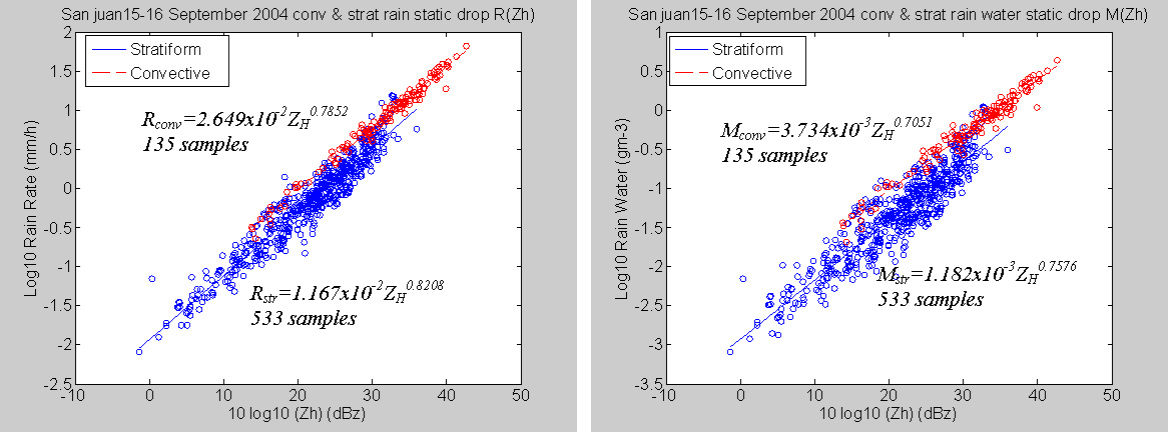

(a) **(b)**

Figure 5-22.Scatter plots of (a) the reflectivity factor Z_H and the rain rate *R*., and (b) the reflectivity factor Z_H and the rain water content *M*. Rain type is classified as stratiform (*str*) and convective (*conv*) using the method described in chapter 4 section 4.2.3.

Z_h depends approximately on the 6th moment of DSD while R depends on the 3.6th moment, this is the principal reason for the variability in Figure 5-22 (a). In addition, Figure 5-22(b) has the same variability but in this case M depends on the 3rd moment of DSD. The results of the least-square regression analysis are shown in Table 5-9 and Table 5-10.

Table 5-9. Coefficients of the $R(Z_H) = cZ_H^b$ rainfall algorithm at X-band wavelength derived from disdrometer data collected during October 2004-July2005 in San Juan, Puerto Rico. R[mmh^{-1}] and Z_H [mm^{6}m^{-3}]. The form log R=b logZ_H + log$c$ was used to obtain $R = cZ_H^b$ relationship.

Rain Type	***c***	***b***
Convective	$2.649x10^{-2}$	0.7852
Stratiform	$1.167x10^{-2}$	0.8208
All	**$9.740x10^{-3}$**	**0.8761**

Table 5-10. Same as in the Table 5-9, but for $M(Z_H) = c'Z_H^{b'}$, where M [gm^{-3}], and Z_H [mm^6m^{-3}]. The form $\log R = b'\log Z_H + \log c'$ was used to obtain $M = c'Z_H^{b'}$ relationship.

Rain Type	***c'***	***b'***
Convective	3.734×10^{-3}	0.7051
Stratiform	1.182×10^{-3}	0.7576
All	**9.25×10^{-4}**	**0.8329**

This analysis does not included error factors as effect of attenuation, radar calibration errors, beam blockage, instrumental noise, etc.

5.2.2.2 Rain rate and rain water content with polarimetric variables

Different combinations of polarimetric variables are possible for constructing rain rate estimators. The obtained regression fits for the R-K_{DP} relation for convective rain, stratiform rain and all rain type were found using the direct fitting of the functional form $R(K_{DP}) = c_1 K_{DP}^{b_1}$ relationship, because for X-Band radar the range for K_{DP} is from 0 to 15 $^\circ km^{-1}$. In order to analyze the variations in DSD, it is important to study the dispersion of plotted samples in the R-K_{DP} diagram in Figure 5-23(a) and in the R-Z_H Figure 5-22(a), concluding that the variations in R-K_{DP} are smaller than in the estimator R-Z_H.

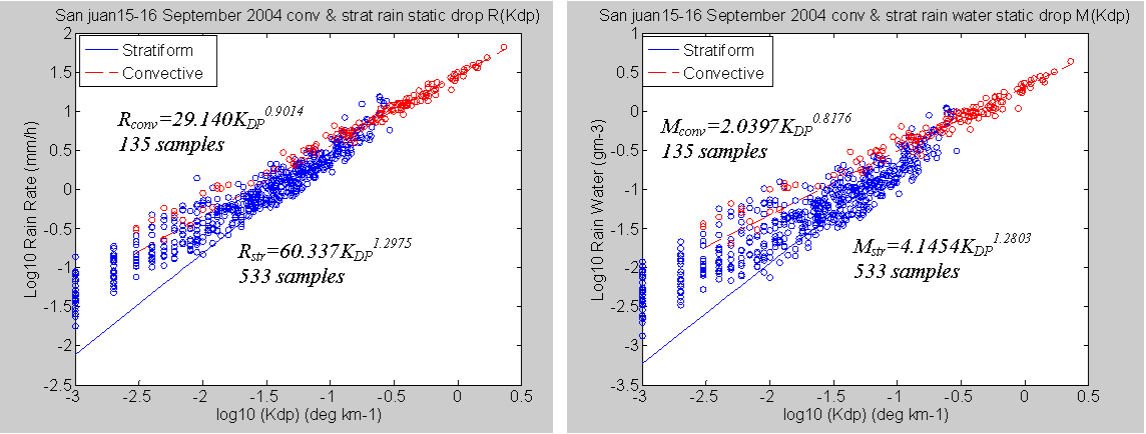

(a) **(b)**

Figure 5-23. Scatter plot of (a) the specific differential phase K_{DP} and the rain rate R, and (b) the specific differential phase K_{DP} and the rain water content M. Rain type is classified as stratiform (*str*) and convective (*conv*) using the method described in chapter 4 section 4.2.3.

Table 5-11. Coefficients of the $R(K_{DP}) = c_1 K_{DP}^{b_1}$ rainfall algorithm at X-band wavelength derived from disdrometer data collected during October 2004-July2005 in San Juan, Puerto Rico. $R \geq 1$ mmh^{-1}. R[mmh^{-1}] and K_{DP} [deg km^{-1}].

Rain Type	c_1	b_1
Convective	29.140	0.9014
Stratiform	60.337	1.2975
All	**29.177**	**0.9272**

Table 5-12. Coefficients of the $M(K_{DP}) = c_1 K_{DP}^{b_1}$ rainfall algorithm at X-band wavelength derived from disdrometer data collected during October 2004-July2005 in San Juan, Puerto Rico. $R \geq 1$ mmh^{-1}. M [gm^{-3}] and K_{DP} [deg km^{-1}].

Rain Type	c_1	b_1
Convective	2.0397	0.8176
Stratiform	4.1454	1.2803
All	**2.0382**	**0.8845**

Table 5-13. Same as in Table 5-11 except for $R(Z_H, Z_{DR}) = c_3 Z_H^{a_3} 10^{0.1 b_3 Z_{DR}}$, where R[mmh^{-1}], Z_H [mm^{6}m^{-3}], and Z_{DR} [dB].

Rain Type	c_3	a_3	b_3
Convective	1.7584x10^{-2}	0.8981	-4.5483
Stratiform	1.0933x 10^{-2}	0.9828	-6.6301
All	**1.103x 10^{-2}**	**0.9864**	**-6.7973**

Table 5-14. Same as in Table 5-12 except for $M(Z_H, Z_{DR}) = c_3 Z_H^{a_3} 10^{0.1 b_3 Z_{DR}}$, where M [gm^{-3}], Z_H [mm^{6}m^{-3}], and Z_{DR} [dB].

Rain Type	c_3	a_3	b_3
Convective	2.164x 10^{-3}	0.855	-3.542
Stratiform	1.081x10^{-3}	0.979	-9.083
All	**1.097x 10^{-4}**	**0.9842**	**-9.314**

5.2.2.3 Comparing results with other locations and estimators

The coefficients found for the relationship $R(Z_H)$ in Puerto Rico are between the coefficients found by Marshall and Palmer and used by NEXRad, as show in Figure 5-24.

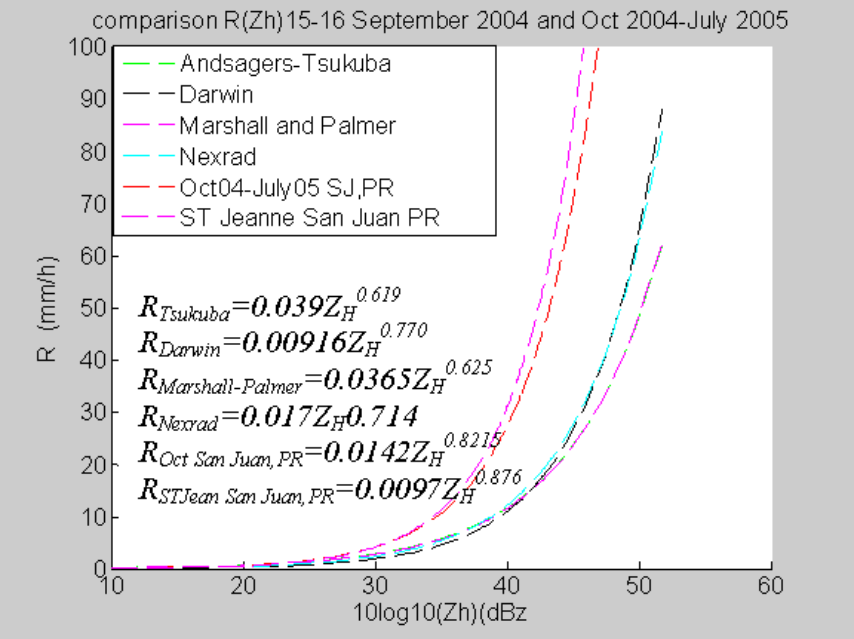

Figure 5-24. The dependence of rain estimator R-Z_H on geografical location or for different axis ratio formulae.

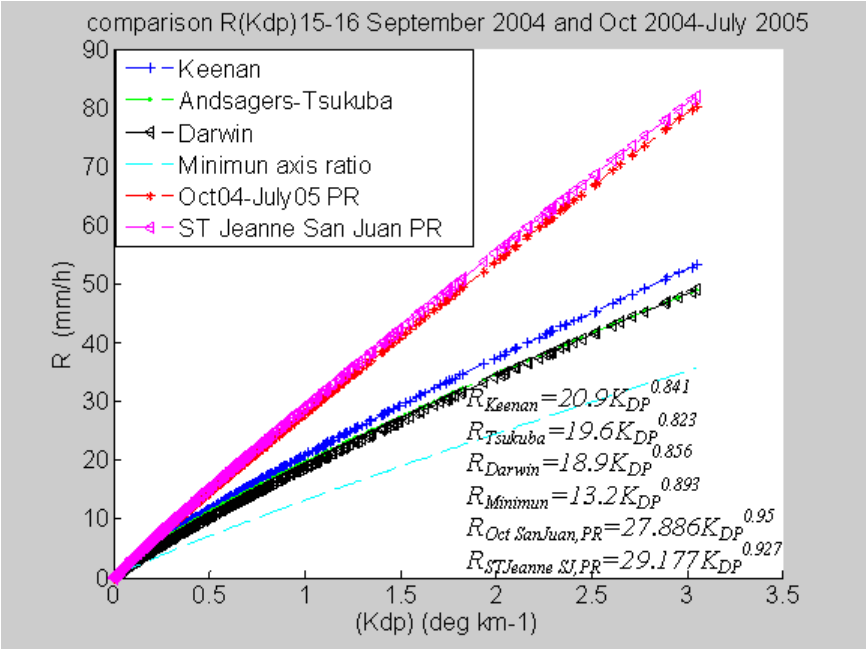

Figure 5-25. The dependence of rain estimator R-K_{DP} on geografical location or for different axis ratio formulae.

5.2.2.4 Estimation error due to DSD variations

Figure 5-26(a, b and c) show comparisons of rain rates R computed for estimators $R(Z_H)$, $R(K_{DP})$, and $R(Z_H, Z_{DR})$ with rain rates R_{dis} calculated from observed raindrop size spectra. From this scatter plots it can be suggested that the worst estimator of the three is $R(Z_H)$, which is most sensitive to variations in DSD. On the other hand, the tendency points to $R(K_{DP})$ as the most accurate estimator from the point of view of the insensitiveness to variations in DSD.

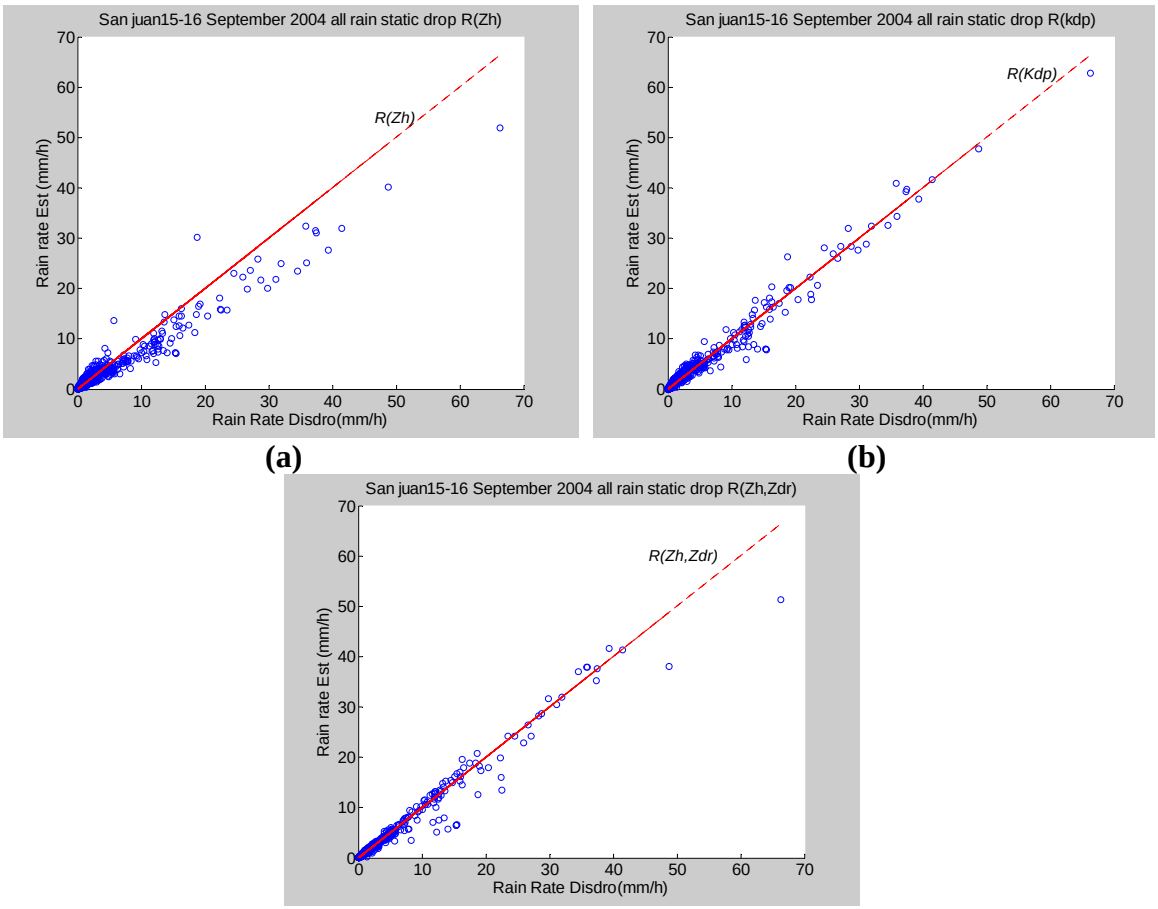

Figure 5-26.Scatter plots of R_{dis} calculated from measured drop size distribution and R estimated by (a) $R(Z_H)$, (b) $R(K_{DP})$, (c) $R(Z_H, Z_{DR})$.

Figure 5-27(a, b, and c) show comparisons of rain water content M computed for estimators $M(Z_H)$, $M(K_{DP})$ and $M(Z_H, Z_{DR})$ with rain water content M_{dis} calculated from observed raindrop size spectra. These scatter plots also suggest that the worst estimator of the three is $M(Z_H)$, while $M(K_{DP})$ tends to be the most accurate from the point of view of the insensitiveness to variations in DSD.

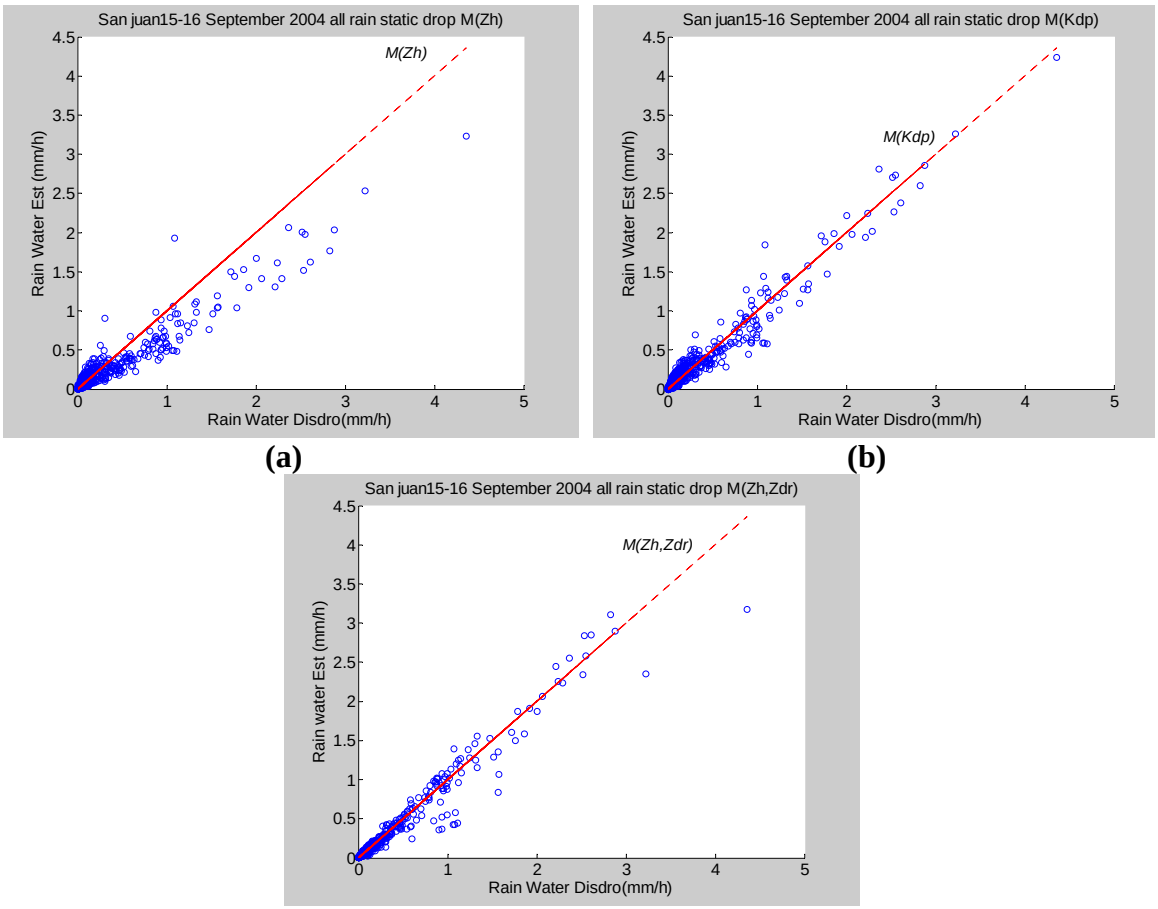

Figure 5-27.Scatter plots of M_{dis} calculated from measured drop size distribution and M estimated by (a) $M(Z_H)$, (b) $M(K_{DP})$, (c) $M(Z_H, Z_{DR})$.

The computed average NEs of $R(Z_H)$, $R(K_{DP})$ and $R(Z_H, Z_{DR})$ for all data samples were 23.39%, 9.34% and 14.53% respectively as it can be seen in Figure 5-28(a). The statistical errors for each estimator of rain water content M due to natural variations in DSD are shown in Figure 5-28(b). The $M(Z_H)$ estimator was clearly the most sensitive variations in the DSD, while $M(K_{DP})$ was the least sensitive.

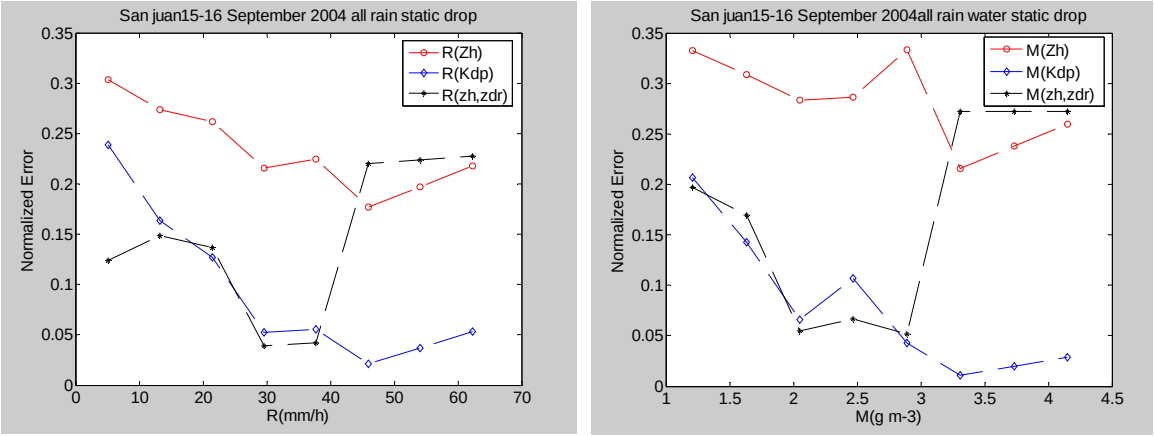

(a) **(b)**

Figure 5-28. Normalized error of three types of (a) rain rate estimators; $R(Z_H)$, $R(K_{DP})$ and $R(Z_H,Z_{DR})$, (b) rain water estimators; $M(Z_H)$, $M(K_{DP})$ and $M(Z_H,Z_{DR})$.

The average PRMSE of $R(Z_H)$, $R(K_{DP})$ and $R(Z_H, Z_{DR})$ for all data samples were 26%, 12% and 16% respectively as it can be seen in Figure 5-29(a). The same statistical errors for each estimator of rain water content M due to natural variations in DSD are shown in Figure 5-29(b).

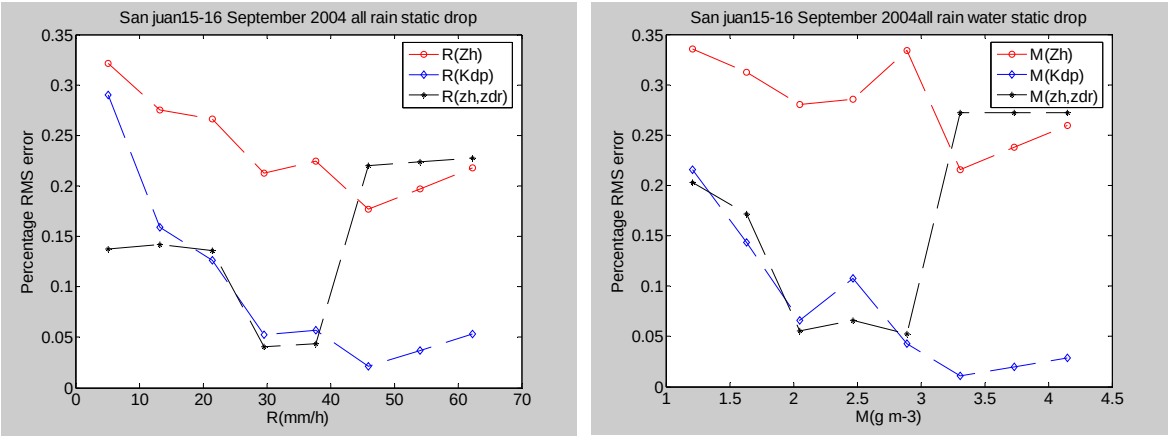

(a) **(b)**

Figure 5-29. Percentage RMS error of three types of (a) rain rate estimators; $R(Z_H)$, $R(K_{DP})$, and $R(Z_H,Z_{DR})$, (b) rain water estimators; $M(Z_H)$, $M(K_{DP})$ and $M(Z_H,Z_{DR})$.

Figure 5-30(a) shows the MRE error of $R(Z_H)$, $R(K_{DP})$ and $R(Z_H, Z_{DR})$. Note that MRE tends to decrease with increasing rain rate. Figure 5-30(b) shows the MRE of the

equivalent *M* estimators. MRE also tends to decrease with increasing rain rate. While the MRE of the classic estimator $R(Z_H)$ for rain rates larger than 10 mm/h is about 140%, the MREs of polarimetric estimators $R(K_{DP})$ and $R(Z_H, Z_{DR})$ for the same rain rate intervals are 115% and 80% respectively. From these comparisons, we can conclude that $R(K_{DP})$ is the least sensitive to variations in DSD.

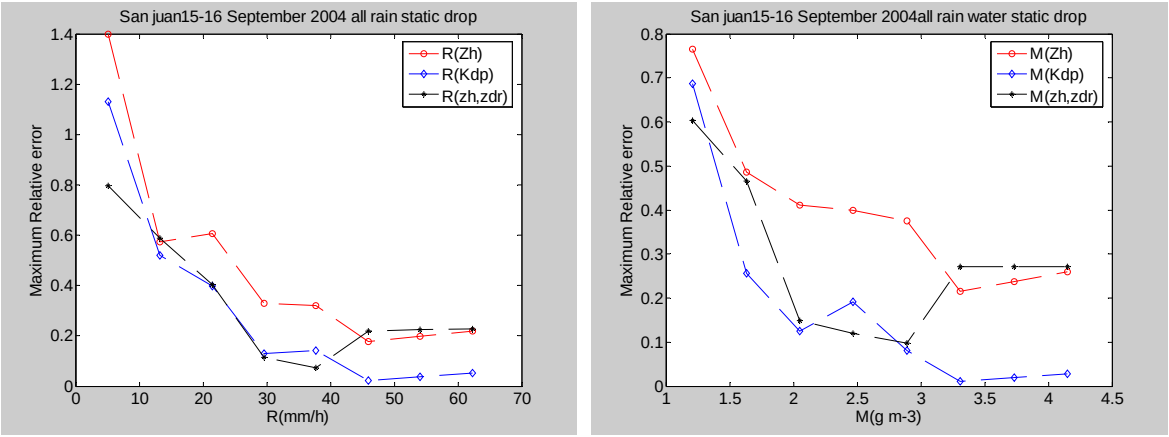

(a) **(b)**

Figure 5-30. Maximum relative error of three types of (a) rain rate estimators; $R(Z_H)$, $R(K_{DP})$ and $R(Z_H,Z_{DR})$, (b) rain water estimators; $M(Z_H)$, $M(K_{DP})$ and $M(Z_H,Z_{DR})$.

5.2.2.5 Effect of unusual DSD on polarimetric rain estimators

The R-K_{DP} method is less sensitive to variations in DSD, and there are several samples where R-K_{DP} method overestimated the rain rate. Figure 5-31 show relative errors of each DSD samples, where the values of R_{est}-R_{dis} greater than 20 mmh^{-1} are samples where rain rate is overestimated, these samples are called 'Unusual', in this case doesn't exist unusual values with this concept.

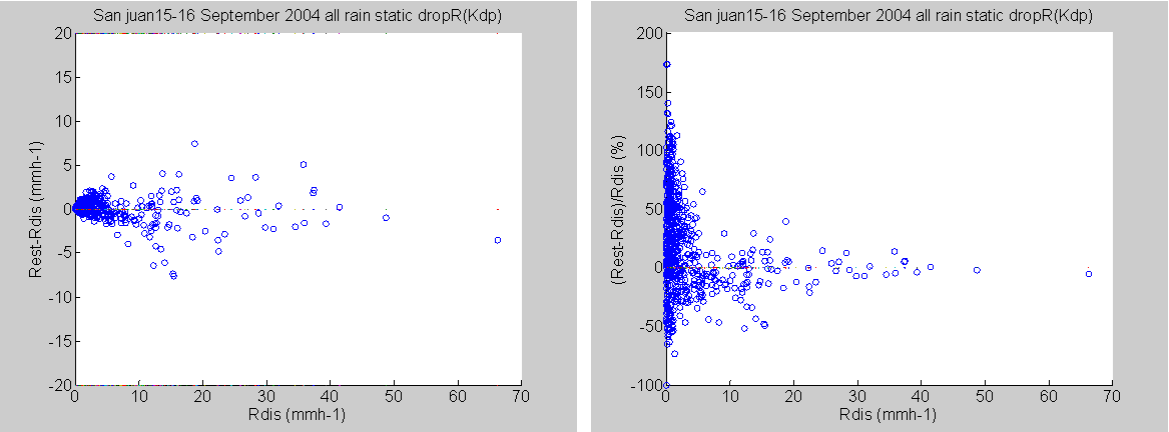

Figure 5-31. Relationship between relative error of $R(K_{DP})$ and R. Samples which have errors larger than about 20 mmh^{-1} are numbered.

Table 5-15. Summary of statistic of gamma DSD parameters for 15th and16th September 2004 collected in San Juan, Puerto Rico.

	$\text{Log}_{10}(N_w)$ (m^{-3} mm^{-1})	D_0 (mm)	Λ (mm^{-1})	μ
Average value	4.4127	0.9183	7.6079	2.8166
Modal value	3.8	0.8	5	1
Standard deviation	4.6145	0.1809	4.9451	3.1950
Central 90 percentile	0.4348~ 0.7048	0.6310~1.2528	2.4932~ 18.4433	-1.5 ~ 9.5

Histogram of gamma DSD parameters are summarized Table 5-15. According to Figure 5-32, DSD parameters are widely distributed: the central percentiles of $\log_{10}(N_w)$, D_0, Λ, and μ are 0.4348~ 0.7048, 0.6310~1.2528, 2.4932~ 18.4433, -1.5 ~ 9.5.

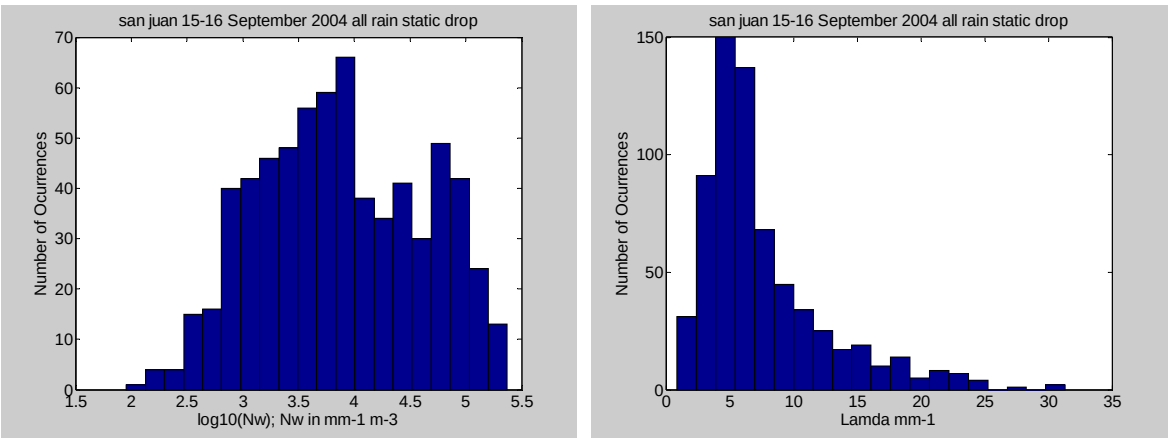

(a) **(b)**

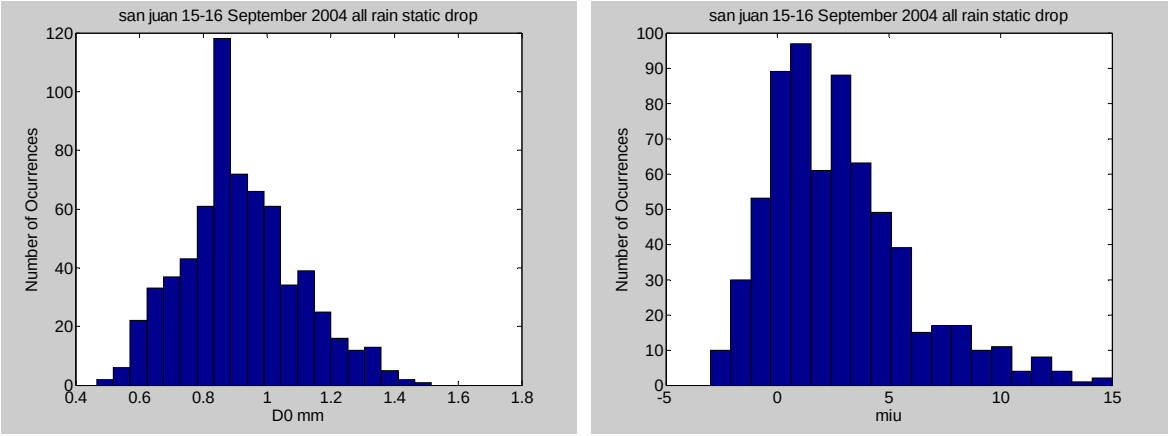

(c) **(d)**

Figure 5-32. Histogram of gamma DSD parameter (a) N_W, (b) Λ, (c) D_0, (d) μ of analyzed data.

5.2.2.6 Further improvement in the accuracy of rain estimators using Z_{DR}

Unfortunately, of the three parameters, only D_0 can be directly related to Z_{DR} by a power law form as shown in Figure 5-33. This fact has been pointed out by several researches. *Seliga and Bringi* (1976) first showed that D_0 was a function of Z_{DR} when the DSD was exponential. Bringi et al (1998) found a D_0-Z_{DR} relationship by analyzing DSD in thunderstorms using an airborne particle imaging sensor. *Maki* et al. (2005) found the flow relationship $D_0=1.59\ Z_{DR}^{0.447}$, in the present study for October 2004-July 2005 found the relationship $D_0 = 1.2559_{DR}^{0.3178}$ as show in Figure 5-18 and for September 15-16, 2004 found the relationship $D_0 = 1.195477 Z_{DR}^{0.2932}$ as show in Figure 5-33.

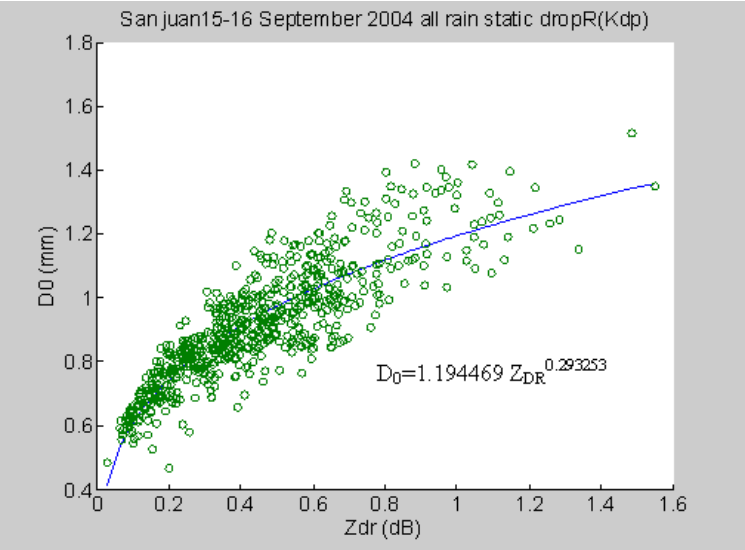

Figure 5-33. Relation between D_0 and Z_{DR}. The blue line shown is least square fitting curve.

5.2.2.7 Potential of X-band polarimetric radar for operations use

Figure 5-34 shows the dependence of the relationship between K_{DP} and R on the wavelength. According to Figure 5-34, the increase in sensitivity of K_{DP} is remarkable at the X-Band wavelength.

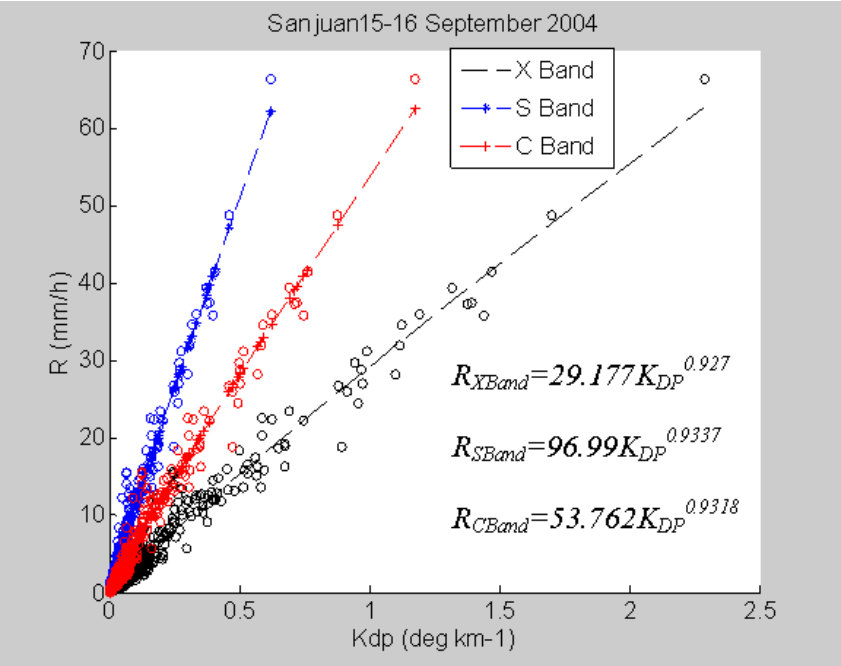

Figure 5-34. Dependence of R-K_{DP} relations on wavelength.

5.3 Drop Size Distribution Characterization

In order to characterize Drop Size Distribution in San Juan, Puerto Rico, the second method for classifying rain type was used. Table 5-16 shows the data used for drop size distribution from October 2004 to July 2005 and Table 5-17 the same but for 15th and 16th September.

Table 5-16.Data quantity and day measured October 2004 July 2005

Date	Convective	Stratiform	Total
V04305, October 31,2004	44	79	123
V04306, November 1,2004	55	75	130
V04348, December 13, 2004	10	12	22
V05037, February 6, 2005	8	14	22
V05101, April 11, 2005	13	20	33
V05108, April 18, 2005	20	47	67
V05109, April 19, 2005	67	50	117
V05110, April 20, 2005	4	38	42
V05111, April 21, 2005	56	26	82

V05133, May 13, 2005	24	17	41
V05136, May 16, 2005	34	40	74
V05137, May 17 2005	19	118	137
V05143, May 23, 2005	13	9	22
V05144, May 24, 2005	11	41	52
V05178, June 27, 2005	23	10	33
V05179, June 28, 2005	45	20	65
V05192, July 11, 2005	23	45	68
V05195, July 14, 2005	15	17	32
Total October 2004 - July 2005	**484**	**678**	**1162**

Table 5-17. Data quantity and day measured 15-16 September, TS Jeanne

Date	**Convective**	**Stratiform**	**Total**
V04259, September 15, 2004	49	185	234
V04260, September 16, 2004	64	116	180
Total September15-16, 2004	**113**	**301**	**414**

Table 5-18 summarizes values found for both $<D_m>$ and $\log_{10}<N_w>$; these were as expected with maritime characteristics, even when convective rain results were not consistent with previous studies made in the Island. These studies will be discussed later.

Figure 5-35 shows results from previous studies on stratiform rain parameters as well as findings from this work in Sept 15th and 16th 2004 and in the period October 2004-July 2005 (see San Juan markers). Regarding stratiform rain, about 72.705% of data points were classified as this type on the 15th and 16th of September, while about 58.35% were selected on October 2004-July2005.

Table 5-18. Dm and log10<Nw>Results Summary

DAY/RAIN TYPE	$<D_m>$ [mm]	$\log_{10}<N_w>$
Sep. 15-16, 2004 stratiform	1.0470	4.1066
Sep. 15-16, 2004 convective	0.9847	4.9783
Oct 2004-July 2005 stratiform	0.9293	4.5562
Oct 2004-July 2005 convective	1.122	5.0061

On the other hand, as opposed to findings by *Ulbrich, Petitididier and Campos* (1999) in a mountainous region of the island, when continental properties were found in the DSDs, log10<N_w> versus <D_m> plot shows characteristics similar to the Maritime Cluster (see Figure 5-36).

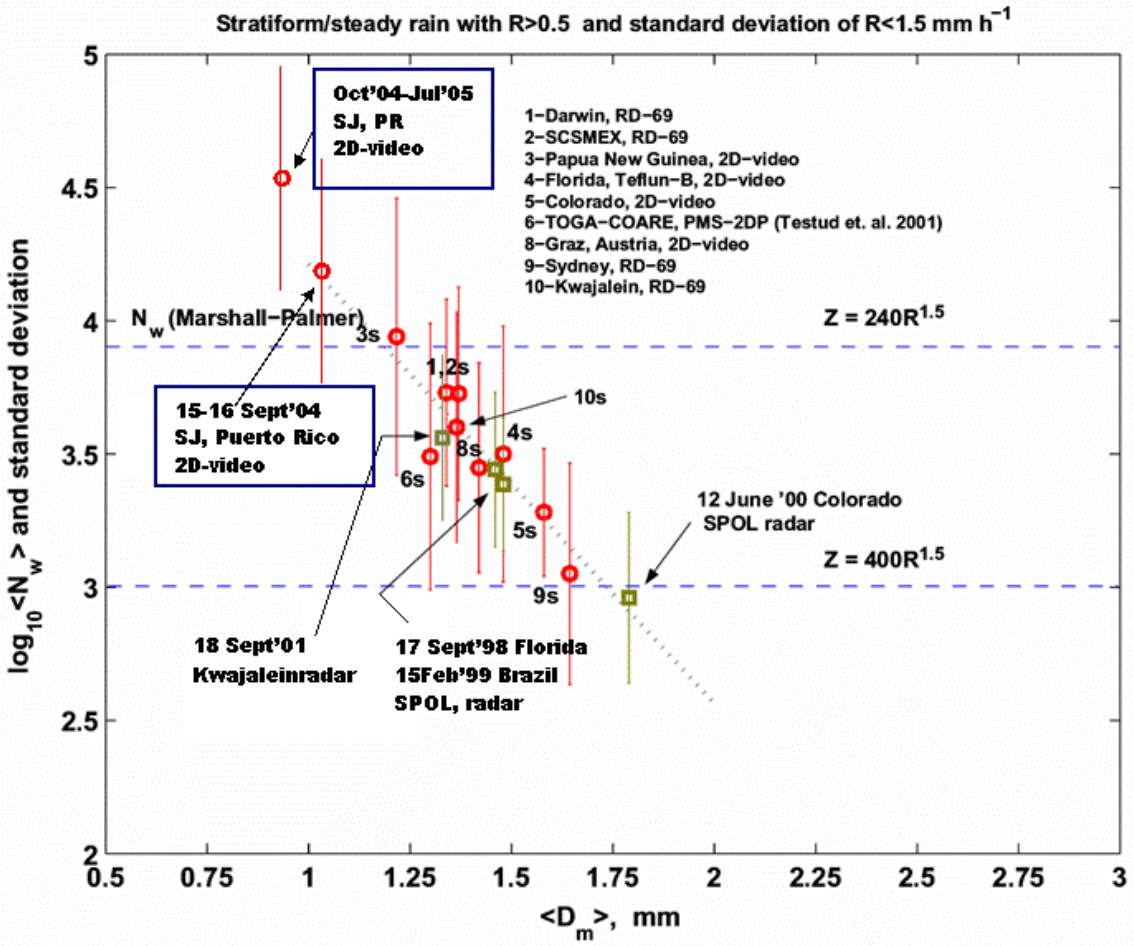

Figure 5-35.The value of log10<N_w> (with 1s std dev bars) versus <D_m> from 2DVD data (numbered open circles) and dual-polarization radar retrievals (open squares as marked) for stratiform rain. Dotted line is the least squares fit. Note that N_w is the 'normalized' intercept parameter and D_m is the mass-weighted mean diameter of a 'normalized' gamma DSD.

As convective rain, about 27.29% of data points were classified as this type on the 15th and 16th of September, while about 41.65% were selected on October 2004-July 2005.

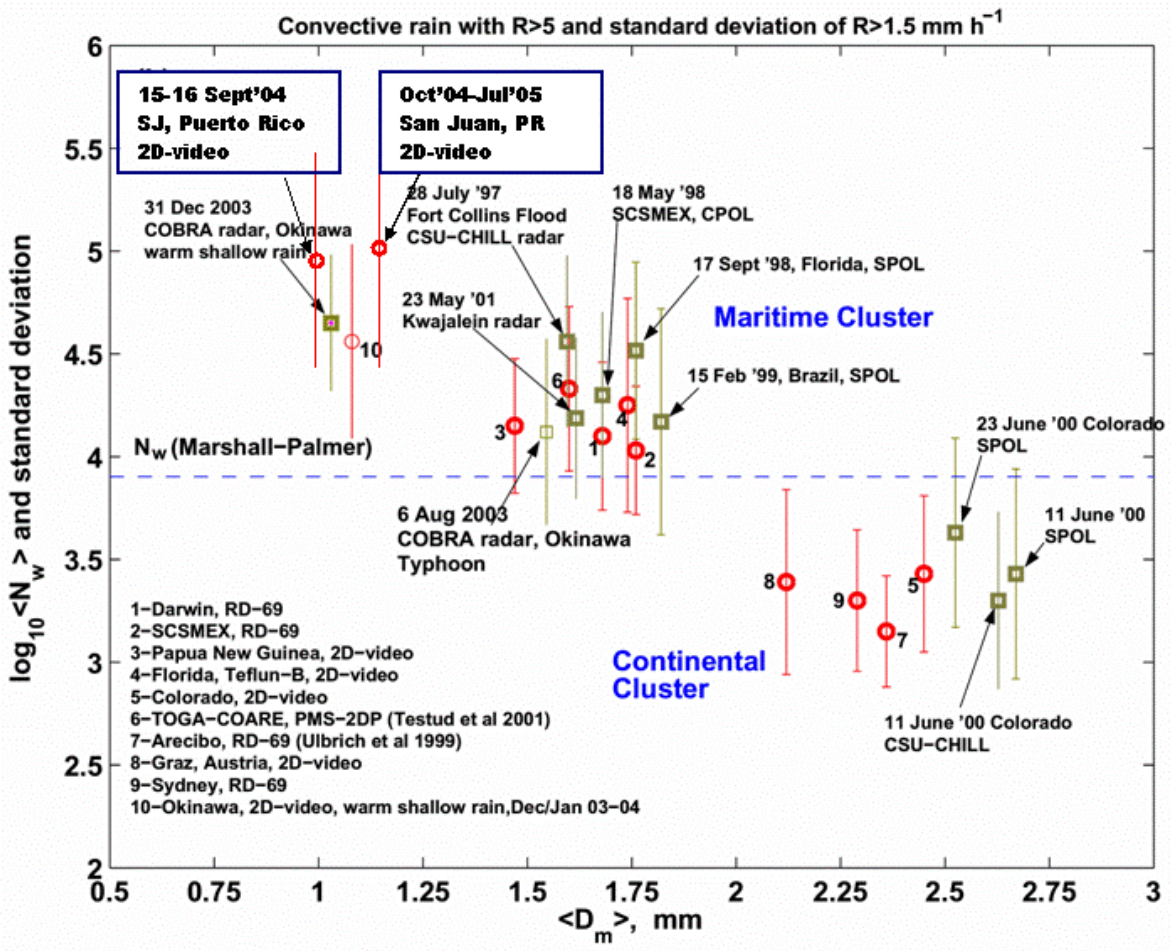

Figure 5-36. As in Figure 5-35 except data for convective rain. Note that N_w is the 'normalized' intercept parameter and D_m is the mass-weighted mean diameter of a 'normalized' gamma DSD.

Next pages present scatter plots (Figure 5-37 to Figure 5-42) characterizing DSDs for the events under consideration.

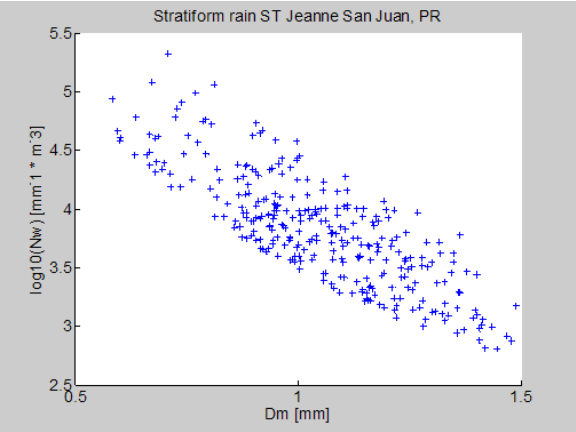

(a)

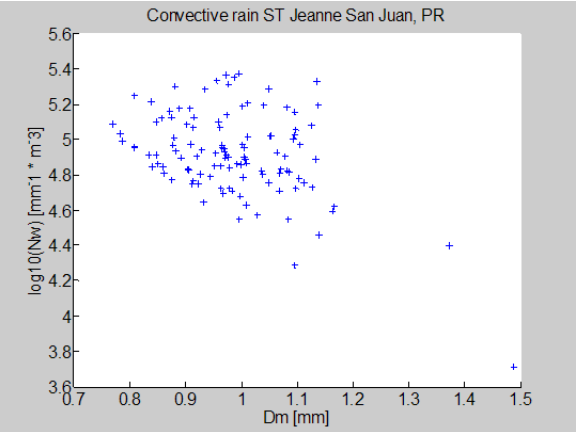

(b)

Figure 5-37. $Log_{10}(N_w)$ vs. D_m scatter plot for the Tropical Storm Jeanne, affecting Puerto Rico on September 15-16, 2004. (a) Stratiform rain type; (b) convective.

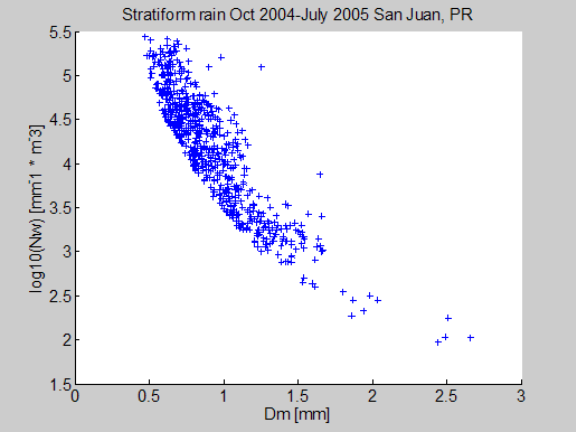

(a)

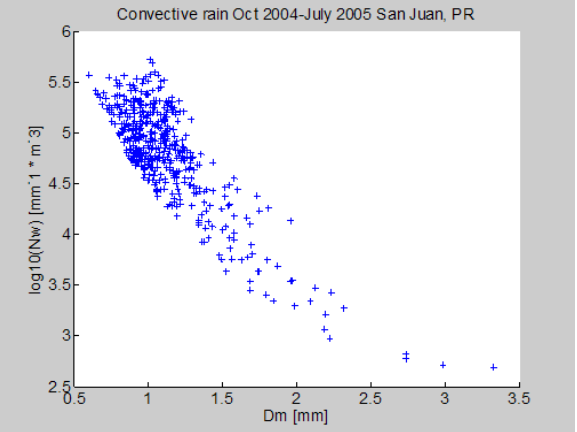

(b)

Figure 5-38. $Log_{10}(N_w)$ vs. D_m scatter plot for period October 2004-July 2005. (a) Stratiform rain type; (b) convective.

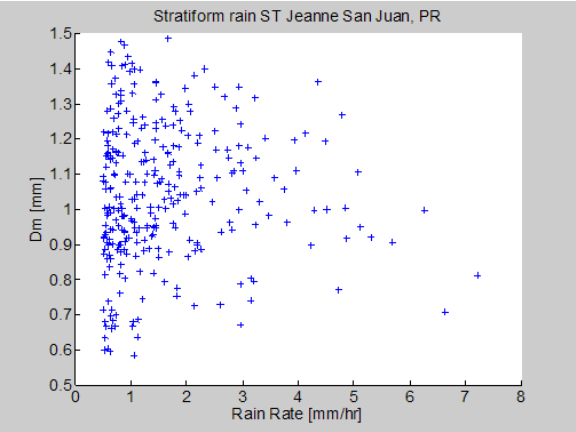

(a)

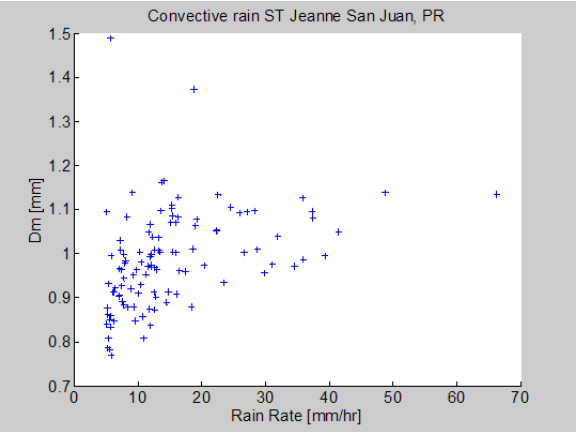

(b)

Figure 5-39. D_m vs. rain rate scatter plot for the Tropical Storm Jeanne, affecting Puerto Rico on September 15-16, 2004. (a) Stratiform rain type; (b) convective.

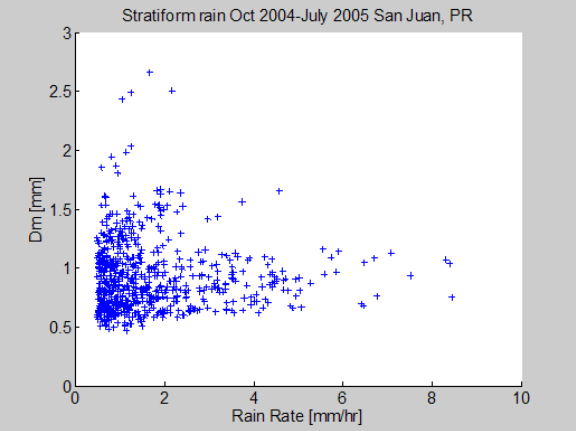

(a)

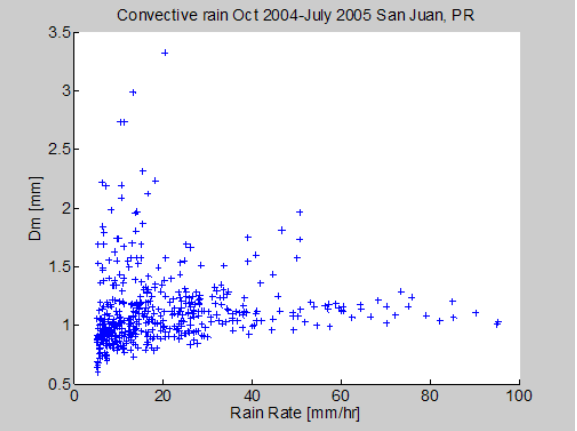

(b)

Figure 5-40. D_m vs. rain rate scatter plot for period October 2004-July 2005. (a) Stratiform rain type; (b) convective.

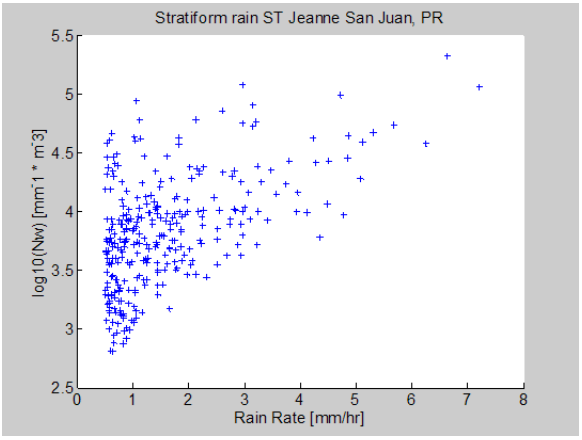

(a)

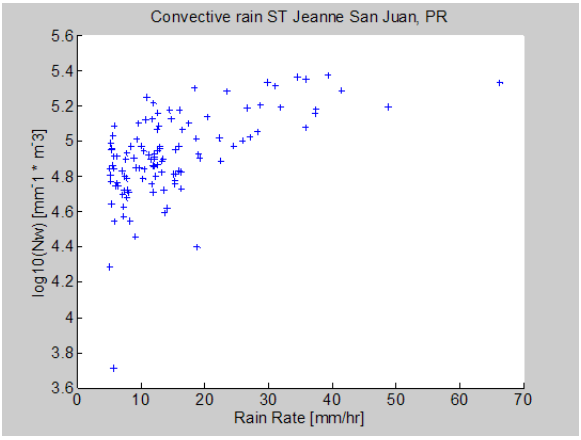

(b)

Figure 5-41. $Log_{10}(N_w)$ vs. rainrate scatter plot for the Tropical Storm Jeanne, affecting Puerto Rico on September 15-16, 2004. (a) Stratiform rain type; (b) convective.

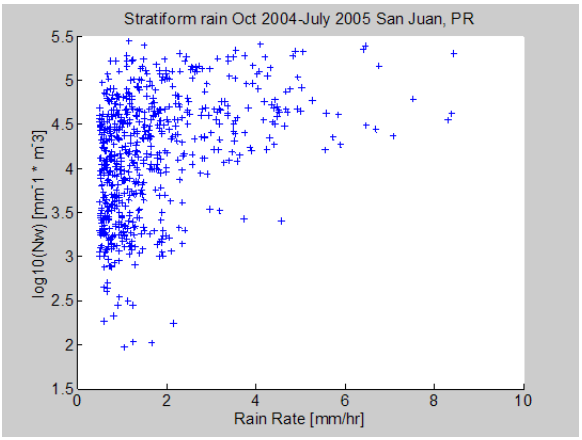

(a)

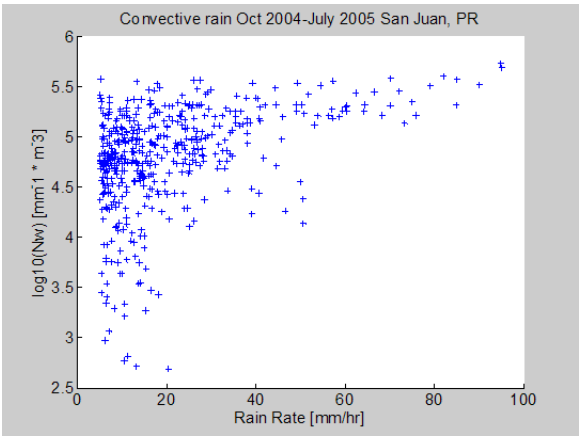

(b)

Figure 5-42. $Log_{10}(N_w)$ vs. rainrate scatter plot for period October 2004-July 2005. (a) Stratiform rain type; (b) convective.

When comparing these results to preliminary results, these confirm disparities in weather types, being at very different geographical areas. Nevertheless N_w results from convective rain, as seen Figure 5-36 tends to approach maritime cluster characteristics, as has happened in other instances in the same area. Therefore we understand DSDs can be highly variable even within the same location.

6 CONCLUSIONS AND FUTURE WORK

The present work quantified the sensitivity of three types of rain rate estimators $R(Z_H)$,$R(K_{DP})$ and $R(Z_H, Z_{DR})$ to natural variations in DSD. Most of previous work on this topic evaluated polarimetric estimators comparing radar estimates with data from surface gauges. Those studies have concluded that the difference between radar estimates and rain gauge data is related to the accuracy of the rain rate estimator to variations in DSD as well as to other factors, such as differences in sampling volume size, differences in observation height, accuracy of radar system calibration, etc. Therefore, the present work utilized T-matrix scattering simulation to exclude factors other than natural variations in DSD. The results of the simulations executed with the present work show that the estimator $R(K_{DP})$ is less sensitive to natural variations in DSD than the classical estimator $R(Z_H)$ for the two events that were analyzed. 'The normalized errors (NEs) of $R(Z_H)$ and $R(K_{DP})$ for October/2004 are 41% and 15% respectively, while for September/2004 they are 23% and 9%. The error tends to decrease with increasing rain rate. For example, at $R>10$ *mm/h* the error of $R(K_{DP})$ due to DSD variations is about one sixth of $R(Z_H)$. Comparison of the R-K_{DP} relationships obtained from DSD samples measured at two different locations (Darwin Australia and Tsukuba, Japan) show that the difference is less than 5%, while comparison of the R-Z_H relationships between Darwin and Tsukuba shows that the average difference without regard for sign is about 77%. These results clearly show that $R(K_{DP})$ is less sensitive to DSD variations compared to $R(Z_H)$ and supports the conclusion of Bringi et al. (2003) over that of Illingworth and *Blackman* (2002) and *Illingwohh* (2003), who mentioned that the R-K_{DP} relationship may have

similar sensitivity to natural variations of DSD as does the R-Z_H relationship. The lower sensitivity of $R(K_{DP})$ and the higher sensitivity of $R(Z_H)$ to variations in DSD can be explained by the fact that the difference between the forward-scattering amplitudes at horizontal (H) and vertical (V) polarizations $f_H(D)$-$f_V(D)$ in the definition of K_{DP} is proportional to the 4.78th power of the diameter of a raindrop for the mono-disperse DSD model, while the reflectivity factor Z_H is proportional to the 6th power of the diameter. As the rain rate and rainwater content are proportional to the 3.67th and the 3rd power of raindrop diameter, respectively, Z_H is more sensitive to variations in DSD than is K_{DP}. It was also shown for an observed DSD spectrum that the contribution pattern of drop diameter to K_{DP} is closer to that of R compared to the contribution pattern to Z_H.

It was found from the analysis of estimation errors that unusual DSDs with extremely large D_0 values decrease the accuracy of $R(K_{DP})$. Further improvement can be attained by the usage of Z_{DR} in rain rate estimators, due to the correlation between D_0 and Z_{DR}. The parameter Z_{DR} can also improve the accuracy of $R(Z_H)$ dramatically. Both the NE and PRMSE of $R(Z_H, Z_{DR})$ are close to the results obtained for $R(K_{DP})$. The improvement of R(Z_H) by considering Z_{DR} is because of the fact that Z_{DR} is a measure of D_0 and the effect of 'unusually' large or small D_0 on the accuracy of $R(Z_H)$ can be cancelled by the form of $R(Z_H, Z_{DR}) = c_3 Z_H^{a_3} 10^{0.1 b_3 Z_{DR}}$, where b_3 is negative.

As shown above, Z_{DR} is a useful parameter in improving rain estimators. However, it is also well know that correction of Z_{DR} for differential attenuation caused by heavy rainfall is indispensable at the X-band wavelength. *Seliga and Bringi* (1976) mentioned that an accuracy of 0.2 dB for Z_{DR} was necessary for the retrieval of raindrop

size distribution. Accuracies of 0.1 dB is necessary for Z_{DR} measurements and of at least 0.5 dB accuracy for Z_H measurements are necessary (*Sachidananda and Zrnic* 1987, *Jameson* 1991) for accurate estimation of rain rates. These requirements for measurement accuracy of Z_H and Z_{DR} have been making it difficult for an estimator of the form $R(Z_H, Z_{DR})$ to be used as an operational estimator. Recently, as shown by *Matrosov* et al. (2002) and *Park* et al. (2005a, b), attenuation correction of Z_H and Z_{DR} is possible using differential phase information at the X-band wavelength and may be used for operational use. However, total evaluation of the algorithm is necessary for X-band polarimetric radar to be able to answer the question of which algorithm or what kind of combination is appropriate for operational purposes. Observations with X-band polarimetric radar have been carrying out by several researchers to evaluate X-band polarimetric radar not only for research purposes but also operational use (*Matrosov* et al. 2002; *Anagnostou* et al. 2004; *Maki* et al.).

Data from NCDC and NWS rain gauges closely corresponded to that of the disdrometer. TRMM data was slightly higher, but this can be due to its low spatial-temporal resolution. Nevertheless, there was agreement in peak values of rain-rates versus time in all the devices.

The RMS error when NCDC was compared with 2DVD was significantly smaller than when NCDC was compared with TRMM, which reveals a greater similarity between NCDC and 2DVD data than with TRMM.

REFERENCES

Anagnostou E.N, M.N. Anagnostou, W.F. Krajewski, A. Kruger, and B.J. Miriovsky, 2004: High Resolution Rainfall Estimation from X-Band Polarimetric Radar Measurements.*J. Hydrometeor.* 5, 110-128.

Andsager, K., K. V. Beard, and N. F. Laird, 1999: Laboratory measurements of axis ratios for large drops. *J. Atmos. Sci.*, 56, 2673–2683.

Battan, L.J., 1973: Radar observation of the atmosphere. Univ.Chicago Press, 324 pp.

Brandes, E. A., G. Zhang, and J. Vivekanandan, 2002: Experiments in Rainfall Estimation with a Polarimetric Radar in Subtropical Environment. *J. Appl. Meteor.*, 41, 674-685.

Brandes, E.A., A.V. Ryzhkov, and D.S. Zrinc, 2001: An evaluation of radar rainfall estimates from specific differential phase. *J. Atmos. Oceanic Technol.*, 18, 363-375.

Bringi, V. N., and V. Chandrasekar, 2001: Polarimetric Doppler Weather Radar Principles and Applications. Cambridge University Press, 636 pp.

Bringi, V. N., and V. Chandrasekar, D.Zrnic, and C.W. Ulbrich, 2003: Comments on "The need to represent raindrop size spectra as normalized gamma distribution for the interpretation of polarimetric radar observations".*J. Appl. Meteor*., 42, 1184-1189.

Collaborative Adaptive Sensing of the Atmosphere (CASA) Engineering Research Center, "Overview" [Online]. Available from http://www.casa.umass.edu

Chandrasekar, V., W. A. Cooper, and V. N. Bringi, 1988: Axis ratios and oscillations of raindrops. *J. Atmos. Sci.*, 45, 1323–1333.

Chandrasekar, V., and V. N. Bringi, 1988: Error structure of multiparameter radar and surface measurements of rainfall. Part X-band attenuation. *J. Atmos. Oceanic Technol*., 5, 796–802.

Chandrasekar, V., and V. N. Bringi, V. N. Balakrishnan, and D. S. Zrnic´, 1990: Error structure

of multiparameter radar and surface measurements of rainfall. Part III: Specific differential phase. *J. Atmos. Oceanic Technol*.,7, 621–629.

Doviak, R. J.and D. S. Zrnic, Doppler Radar and Weather Observations, Second edition, Academic Press, San Diego, 1993.

Federal Aviation Administration [Online]. Available from http://faa.gov/asos/

Goddard, J. W. F., and S. M. Cherry, and V. N. Bringi, 1982: Comparison of dual-polarized radar measurements of rain with ground-based disdrometer measurements. *J. Appl. Meteor*., 21, 252–256.

Goddard, J. W. F., and S. M. Cherry, 1984: The ability of dualpolarization radar (copolar linear) to predict rainfall rate and microwave attenuation. *Radio Sci*., 19, 201–208.

Jameson, A. R., 1991: A comparison of microwave techniques for measuring rainfall. *J. Appl. Meteor.*, 30, 32–54.

Jameson, A. R., 1994: An alternative approach to estimating rainfall rate by radar using propagation differential phase shift. *J. Atmos. Oceanic Technol*., 11, 122–131.

Keenan, T. D., L. D. Carey, D. S. Zrnic´, and P. T. May, 2001: Sensitivity of 5-cm wavelength polarimetric radar variables to raindrop axial ratio and drop size distribution. *J. Appl. Meteor*., 40, 526–545.

Kruger, A., W.F. Krajewski, "Two-Dimensional Video Disdrometer: A description," *Journal of Atmospheric and Oceanic Technology*, Vol. 19, pp. 602-617, 2001

Maki M. and V.N.Bringi, 2004: Effect of natural Variations in Rain Drop size Distributions on Rain Rate Estimators of 3 cm Wavelength Polarimetric Radar. *J. Meteor. Soc.Japan*.

Maki, M.,S.G. Park, V.N. Bringi, 2005: Effect of natural variations in rain drop size distributions on rain rate estimatorsnof 3 cm wavelength polarimetrc radar. *J.Meteor. Soc. Japan*.

Matrosov, S. Y., R. A. Kropfli, R. F. Reinking, and B. E. Martner,1999: Prospects for measuring rainfall using propagation differential phase in X- and Ka-radar bands. *J. Appl. Meteor*., 38,766–776.

Matrosov, S.Y., K.A. Clark, B.E. Martner, and A. Today, 2002:X-band polarimetric radar measurements of rainfall. *J. Appl. Meteor*., 41, 941-952.

National Climate Data Center [Online]. Available from http://www.ncdc.noaa.gov/servlets/ULCD

Oguchi, T and Y. Hosoya, 1974: Differential attenuation and differential phase shift of radio waves due to rain: Calculations of microwave and millimeter wave regions. *J. Rech. Atmos*., 8, 121-128.

Sachidananda, M., and D.S. Zrnic, 1987: Rain rate estimates from differential polarization measurements. *J. Atmos. Oceanic Technol*., 4, 588-598.

Seliga T.A. and V.N. Bringi, 1976: Potential use of radar differential reflectivity measurements at orthogonal polarizations for measuring precipitation. *J. Appl Meteor*., 15, 69-76.

Schönhuber, M. et al., "Weather Radar versus 2D-Video-Distrometer Data," *Proceedings of the III International Symposium on Hydrological Applications of Weather Radars*, São Paulo, Brazil, August 20-23, 1995.

Schönhuber, M., "Distrometer results obtained in various climates and their application to weather radar data inversion," *ESA SP-444 Proceedings, Millennium Conference on Antennas & Propagation*, Davos, Switzerland, April 9-14, 2000.

Tan, J., A. R. Holt, A. Hendry, and D. H. O. Bebbington, 1991: Extracting rainfall rates from X-band CDR radar data by using differential propagation phase shift. *J. Atmos. Oceanic Technol.*,8, 790–801.

TRMM Online Visualization and Analysis System (TOVAS) [Online]. Available from http://lake.nascom.nasa.gov/tovas/3B42RT/index2.shtml

Vivekanandan, J., D. N. Yates, and E. A. Brandes, 1999: The influence of terrain on rainfall estimates from radar reflectivity and specific propagation phase observations. *J. Atmos. Oceanic Technol*., 16,837–845.

Zrnic´, D. S., and A. V. Ryzhkov, 1996: Advantages of rain measurements using specific differential phase. *J. Atmos. Oceanic Technol*., 13, 454–464.

Zrnic´, D. S., T. D. Keenan, L. D. Carey, and P. May, 2000: Sensitivity analysis of polarimetric variables at a 5-cm wavelength in rain. *J. Appl. Meteor*., 39, 1514–1526.